Effects of growth feedback on gene circuits: A dynamical understanding

Ling-Wei Kong, Wenjia Shi, Xiao-Jun Tian, Ying-Cheng Lai ✉

School of Electrical, Computer and Energy Engineering, Arizona State University, Tempe, AZ 85287, USA • Department of Physics, Xi'an University of Technology, Xi'an 713300, China • School of Biological and Health Systems Engineering, Arizona State University, Tempe, AZ 85287, USA • Department of Physics, Arizona State University, Tempe, Arizona 85287, USA

Abstract

The successful integration of engineered gene circuits into host cells remains a significant challenge in synthetic biology due to circuit-host interactions, such as growth feedback, where the circuit influences cell growth and vice versa. Understanding the dynamics of circuit failures and identifying topologies resilient to growth feedback are crucial for both fundamental and applied research. Utilizing transcriptional regulation circuits with adaptation as a paradigm, we systematically study 435 distinct topological structures and uncover six categories of failures. Three dynamical mechanisms of circuit failures are identified: continuous deformation of the response curve, strengthened or induced oscillations, and sudden switching to coexisting attractors. Our extensive computations also uncover a scaling law between a circuit robustness measure and the strength of growth feedback. Despite the negative effects of growth feedback on the majority of circuit topologies, we identify a few circuits that maintain optimal performance as designed, a feature important for applications.

> **eLife assessment**
>
> This **valuable** study focuses on the impact of growth feedback on the performance of artificial gene circuits capable of achieving adaptive responses, an **important** problem in synthetic biology. Through **solid** computational analysis, the authors identify specific failure mechanisms, as well as core topologies associated with robust performance based on systematic analysis of over four hundred circuit topologies. The results will be of interest to those working on engineering gene circuits for diverse applications.

Introduction

In biomedical science and engineering, artificially designed gene circuits are anticipated to play an ever-increasing role in disease diagnosis and therapy (*Riglar and Silver, 2018* ↗; *Sedighi et al., 2019* ↗; *Xia et al., 2019* ↗). Gene circuits also show great potential in various applications such as microbiome modulation (*Foo et al., 2017* ↗; *Lee et al., 2018* ↗) and biological containment

(*Gomaa et al., 2014*; *Caliando and Voigt, 2015*). While most gene circuits are designed to function after they are inserted or embedded into host cells, the interactions between the circuit and the host environment are generally extremely complex and can lead to undesired effects that were not present in the original, isolated circuit (*Tan et al., 2009*; *Ceroni et al., 2015*; *Borkowski et al., 2016*; *Ceroni et al., 2018*; *Darlington et al., 2018*a,b; *Gouda et al., 2019*; *Zhang et al., 2021*, *2020*; *Melendez-Alvarez et al., 2021*). Understanding the interactions and identifying the circuit topological structures that can withstand the interactions and thrive in the host are thus of fundamental importance, requiring interdisciplinary efforts among systems and synthetic biology, metabolic engineering, nonlinear dynamics and complex systems.

Typical circuit-host interactions include metabolic burden, cell growth, and resource relocation or competition, among which growth feedback is the most common type of circuit-host interaction between the circuit gene expressions and cell growth. More specifically, a synthetic gene circuit embedded in a host cell possesses an intrinsic coupling mechanism: the circuit affects cell growth and the growth in turn modifies the gene expressions in the circuit (*Klumpp et al., 2009*; *Klumpp and Hwa, 2014*; *Boo et al., 2019*; *Scott et al., 2010*) - the so-called growth feedback. Studies have shown that the growth-mediated feedback can endow a synthetic gene circuit with various emergent properties, such as innate growth bistability (*Deris et al., 2013*). For example, a non-cooperative positive autoregulation system, when coupled with growth feedback, gains increased effective cooperativity, thereby resulting in bistability (*Tan et al., 2009*; *Nevozhay et al., 2012*). In another example, toxin cooperativity can be induced in multiple toxin-antitoxin systems by growth-mediated feedback (*Feng et al., 2014*). The number of steady states in one gene circuit also depends on growth feedback and resource availability (*McBride and Del Vecchio, 2020*; *Melendez-Alvarez and Tian, 2022*). In general, growth feedback acts to hamper the forward engineering of the circuit functions by introducing modes of nonmodularity and reducing the predictability of the circuit components in an in-vivo context. While various phenomena caused by growth feedback were studied with desirable or undesirable effects on the functions of the gene circuits, a systemic picture is lacking on what effects growth feedback can have on the gene circuits, including failures.

A recent study has revealed that growth feedback can have drastically different effects on congruent circuits with distinct topologies (*Zhang et al., 2020*). In particular, the dynamical behaviors of two bistable synthetic memory circuits were studied: a self-activation switch incorporating positive autoregulation and a toggle switch incorporating double-negative regulatory motifs. It was found that growth feedback impacts both circuits but with quite different manifestations. For the toggle switch, memory can be retained and the circuit tends to be refractory towards growth feedback. However, for the self-activation switch, growth feedback leads to memory loss. While these results indicate that the circuit topology can play a significant role in the circuit functions when growth feedback is present, they were obtained through two specific circuit topologies. Since a particular function of the gene circuit can often be achieved by a finite set of core topologies, it is of fundamental interest to identify the most robust topologies in response to growth feedback. The so-identified optimal topologies can then be used to construct synthetic gene circuits capable of maintaining the essential functions to meet the design goals under the fluctuating growth conditions of the host cell. A systematic study of the interplay between the gene circuit topology and growth feedback is needed.

Adaptation is an important and widely studied functionality of gene circuits, which is defined as the ability of the system to respond to environmental changes and to return to the basal or near-basal state after some time (*Knox et al., 1986*; *Tyson et al., 2003*; *Friedlander and Brenner, 2009*; *Ferrell Jr, 2016*). Previously, it was found that certain circuits possess biochemical adaptation (*Ma et al., 2009*) if they contain at least one of the two architectural classes: an incoherent feed-forward loop with a proportion node and a negative feedback loop with a buffering node. A number of synthetic gene circuits were proposed or constructed to achieve adaptation (*Kim et al., 2014*; *Briat et al., 2016*; *Aoki et al., 2019*). Quite recently, a design

principle for circuits with four genes was uncovered for simultaneously achieving noise attenuation and adaptation: the circuit must have a sequential assembly structure (*Qiao et al., 2019* ⧉). However, these existing adaptation studies did not include any growth feedback mechanism.

In this paper, we conduct a comprehensive computational study to uncover and understand the effects of growth feedback on the gene circuits. Specifically, we focus on a type of transcriptional regulation circuit designed for adaptation. There are 425 possible circuit structures (identified by previous research (*Shi et al., 2017* ⧉)), and we study all of them to simulate and test their response under different levels of growth feedback. Altogether, 2×10^5 sets of circuit parameters are randomly sampled for each structure. Our results reveal a vast number of cases where growth feedback has a detrimental effect on circuit function (1.3×10^5 cases in total) with varying response curves and dynamical behaviors. To gain a more intuitive overall picture, we classify these cases into several distinct categories based on the circuits' dynamic behavior. We then systemically summarize the dynamical mechanism behind these growth-induced circuit malfunctions. To quantify circuit adaptation in the presence of growth feedback, we propose a robustness measure that enables us to identify an optimal group of circuits that exhibit a high level of robustness against growth feedback, making them particularly promising for real-world implementation. The motifs associated with this optimal group are found through machine learning. We also obtain a scaling law governing the dependence of this measure on the level of growth feedback and provide a mathematical analysis to gain insights into the underpinnings of the scaling law. The take-home message is that, in spite of the negative effects of growth feedback in the majority of the circuits, there exists a small set of circuits that are still able to deliver optimal performance as designed, which is promising for real-world implementation.

Results

A systemic search of functional failures due to growth feedback

Adaptation is referred to as the ability of a gene circuit to respond to changes in input and then to return to the pre-stimulus output level, even when the input change persists (*Ma et al., 2009* ⧉). More precisely, with an input signal switched from a lower value I_1 to a higher value I_2, as demonstrated in **Fig. 1(b)** ⧉ , a circuit with functional adaptation should have the following response-curve criteria: (i) precision - the final state O_2 should be close to the initial state O_1, (ii) sensitivity - there should be a relatively high O_{peak} in response to the change in the input, and (iii) the system should reach equilibrium within a reasonable relaxation time. A three-node gene circuit can achieve adaptation (*Ma et al., 2009* ⧉), with one node receiving the input (node A), another node realizing various regulatory roles (node B), and a third node outputting the response (node C). A representative circuit topology is shown inside the red dashed box in **Fig. 1(a)** ⧉ . We restrict our study of the class of transcriptional regulatory networks (TRNs) with the AND logic.

In our work, we use a parameter k_g to control the strength of growth feedback, which is a parameter determining the maximal growth rate of the host cells, as mathematically explained in Model description. With all the other parameters fixed, a larger k_g implies a faster cell growth rate and a stronger impact of growth feedback. Previous research identified 425 different three-node TRN network topologies that can achieve adaptation in the absence of growth feedback (*Shi et al., 2017* ⧉), providing the base of our computational study. These topologies can be classified into two families based on the mechanism they rely on to achieve adaptation: networks with a negative feedback loop (NFBL) and networks with an incoherent feed-forward loop (IFFL) (*Shi et al., 2017* ⧉). To investigate the effect of growth feedback on these circuits, we systematically simulate the response of the 425 network topologies under a switch in the input signal. A three-node gene circuit subject to growth feedback has a large number of parameters, which determine the properties of the regulation links within the circuit and the circuit dynamics. For each
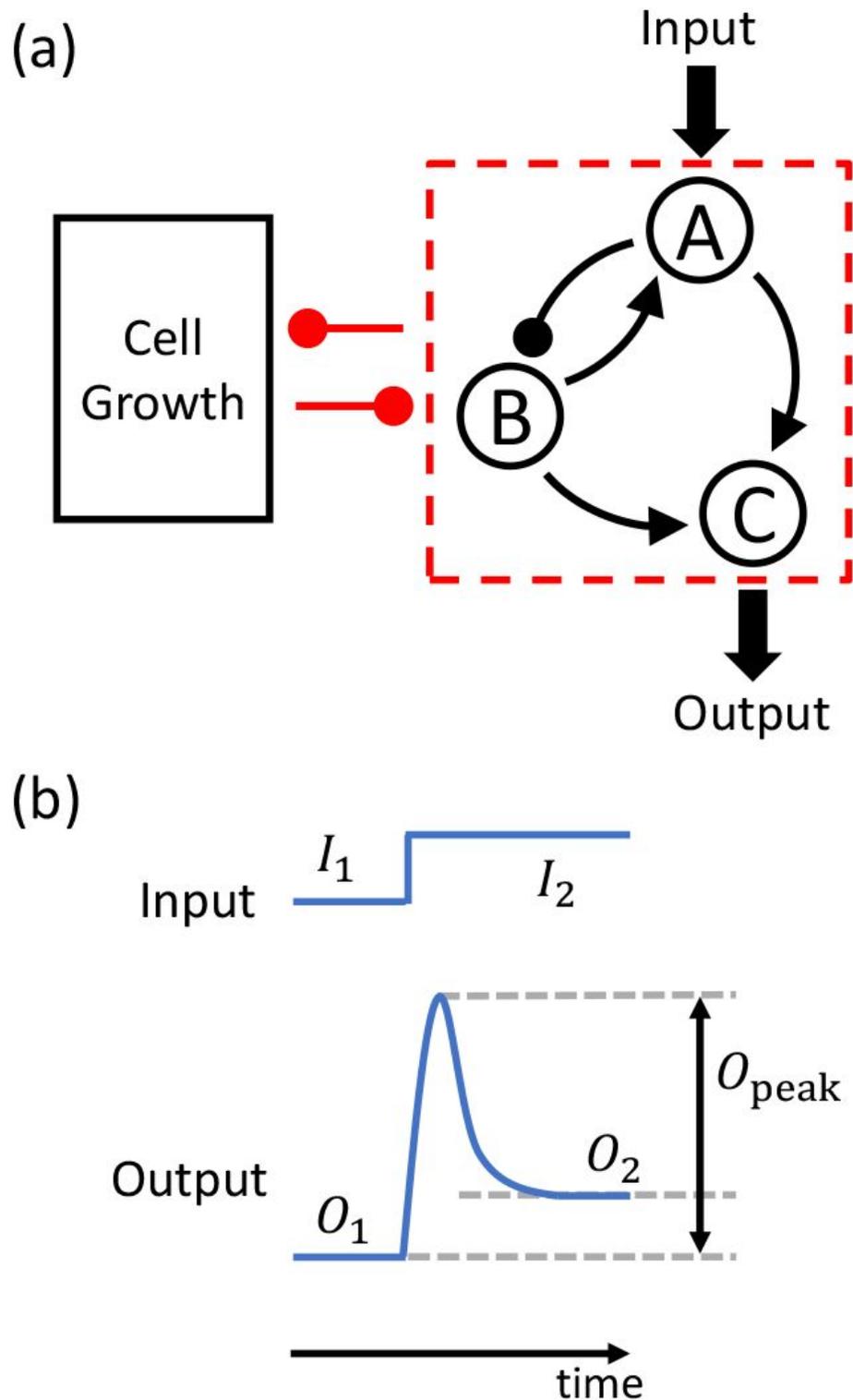
Figure 1.

Schematic illustration of a synthetic gene circuit embedded in a host cell. (a) A representative three-gene circuit (inside the dashed red box) and its dynamical interplay with host-cell growth. Arrows with triangular ends and round ends denote activating and inhibiting regulations, respectively. Altogether, there are 16,038 possible three-node topologies, with 425 topologies capable of adaptation.(b) An example of the circuit input and output signals. The input is an idealized step function of currents I_1 and I_2 before and after the jump, respectively. The output signal is a response of the circuit to the step function. The features of the output signal, as characterized by three key quantities characterizing the signal: O_1, O_2, and O_{peak}, can be used to determine if the circuit has succeeded or failed in its intended function.

topology, we randomly sample 2×10^5 trials of circuit parameters. Altogether, our study involves analyzing approximately 8.5×10^7 different circuits. We find that among these trials, only about 1.5×10^5 meet the adaptation criterion in the absence of growth feedback. For these functional trials, we vary the growth feedback parameter k_g with a series of values, and find that the majority of trials (1.3×10^5 trials, about 87%) lose their adaptation in the interval of $k_g \in (0, 1)$, while only 13% of trials remain functional at $k_g = 1.0$.

A systemic classification of functional failures due to growth feedback

An essential step towards understanding the detrimental or even destructive effects of growth feedback on circuit functioning is to identify the distinct failure scenarios. Our extensive simulations have yielded a comprehensive picture of these scenarios, as shown in **Fig. 2** ⧉. Overall, we have identified six failure scenarios that encompass more than 99.6% of the 1.3×10^5 failing cases we collect. The first level of classification distinguishes between failures that occur continuously or abruptly as the growth-feedback strength k_g increases. In a continuous failure, the response curve deforms continuously as k_g increases, as exemplified in **Figs. 2(a-c)** ⧉. In an abrupt failure, the response curve exhibits a sudden change as k_g increases through a critical value, as illustrated in **Figs. 2(d-f)** ⧉. At the next classification level, we further divide the failures into three types of continuous failures and three types of abrupt failures.

The three types of continuous failures, denoted as types I-III as illustrated in **Figs. 2(a-c)** ⧉, are determined according to the specific quantitative criteria in the response curve that the circuits violate. Type-I continuous failures, as shown in **Fig.2(a)** ⧉, are associated with the violation of the precision criterion. A circuit is deemed as precise if a change in the input signal (e.g., from I_1 to I_2) generates two opposite dynamical effects in the circuit that cancel each other out after a transient and return the final output to the original state, i.e. $O_2 \approx O_1$. For example, in some networks [e.g., the network in **Fig. 1(a)** ⧉], an increase in the input signal I will result in an increase in the concentration of gene A and a reduction in the concentration of gene B. As both genes regulate the output gene C with the respective activation links, for proper system parameter values, the two effects will cancel each other out, resulting in $O_2 \approx O_1$. Type-I continuous failures constitute the largest failure category among all possible circuit topologies, suggesting that the exact cancellation is fragile and the loss of precision is the most common dynamical mechanism behind growth-feedback-induced failures.

Our simulations reveal that an exact cancellation between the two opposite sources at $k_g = 0$ prevents an exact cancellation at any other values of k_g. That is, the set of circuit parameter values leading to perfect precision, in general, depends on the value of k_g (see **Appendix 1** ⧉ for more details). The implication is that, for fixed circuit parameter values, achieving high precision under growth feedback ($k_g > 0$) is difficult if the circuit is precise in the absence of growth feedback ($k_g = 0$).

Type-II continuous failures are characterized by a continuous change in the peak of the response curve, denoted as O_{peak}, as k_g increases, eventually falling below a threshold, as shown in **Fig. 2(b)** ⧉. This type of failure can make it challenging for downstream circuits to detect the peak signal, hindering information transmission in the larger system. Type-II failures are the second most common type of failure observed in our simulations. The occurrence of a high peak in the response curve requires a significant transient deviation from the final equilibrium point. In the presence of growth feedback, the transient behavior changes, which can further alter the peak height O_{peak}.

Type-III and type-IV failures arise due to growth-feedback-induced oscillations, while type-V and type-VI failures are caused by bistability or bifurcations, with fold bifurcations being the most common type. To provide a more detailed understanding of these different failure scenarios, we
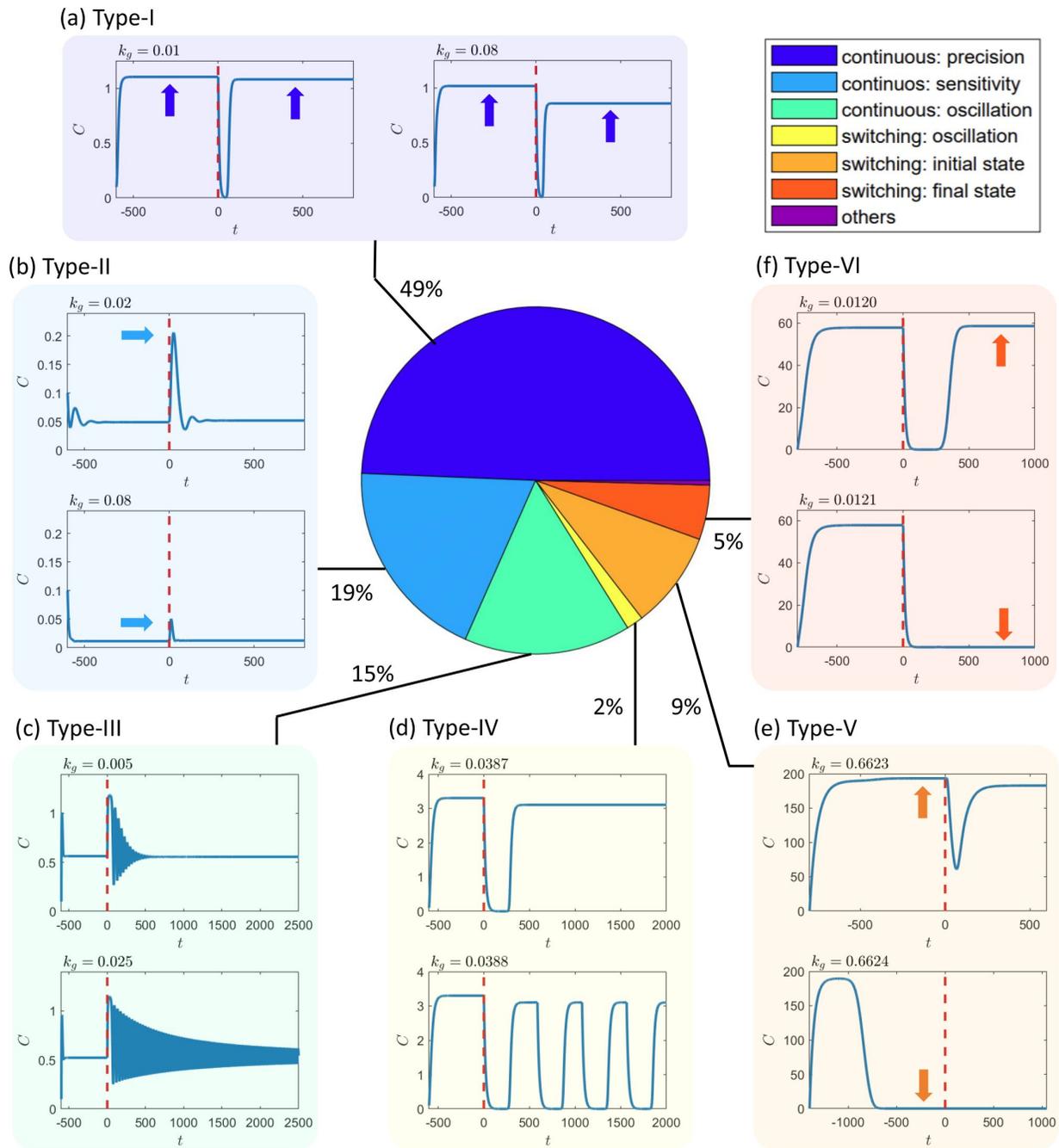
Figure 2.

Systemic classification of circuit failure scenarios due to growth feedback. This study identifies six computationally detectable categories of failures based on the criterion of functional adaptation that the circuit violates as the effect of growth feedback becomes stronger. (a) Type-I and (b) type-II failures correspond to the cases where the precision criterion or sensitivity criterion is violated in a continuous fashion as the growth-feedback strength k_g increases, respectively. (c) Type-III and (d) type-V failures occur when the circuits lose adaptation due to growth-feedback-induced oscillation, either continuously or abruptly, as k_g increases, respectively. The abrupt changes in type-V are caused by bifurcations, mostly a saddle-node bifurcation of cycles or an infinite-period bifurcation. For instance, the case shown in (d) undergoes an infinite-period bifurcation. (e) Type-V and (f) type-VI failures are when the circuits lose adaptation due to an abrupt change in O_1 or O_2 as k_g increases, respectively, which are caused by bistability or bifurcations in the systems. Trials that are not categorized under these six classifications or fall into multiple categories constitute less than 0.4% of all cases (see text for more details and discussions about each failure class). The insets around the pie chart provide exemplary response curves of the circuits in each failure scenario. Each inset shows the concentration of the output node C versus time with two values of the growth-feedback strength k_g, one below and another above the failure threshold, for the specific failure scenario. In each case, the input is switched from state I_1 to state I_2 at the time indicated by the red vertical dashed line.

discuss the two mechanisms, respectively, in the sections of Growth-feedback induced oscillations and Bistability and bifurcations below.

Box 1.

Three classes of growth-induced failures

All the failures we observed can be categorized into the following three general classes, applicable to both the three-gene and four-gene circuits we tested:

Continuous Deformation of the Response Curve Typically, we require a specific range of response curve shapes for a gene circuit, such as a peak in the output with a minimum height or duration. In a failure caused by continuous deformation, the growth feedback prompts a gradual change that crosses the boundary of these criteria for response curve shapes.

Growth-Induced or Growth-Strengthened Oscillations Growth feedback can induce oscillations in a circuit through various types of bifurcations or amplify existing oscillatory behavior with longer relaxation times or larger amplitudes. A circuit experiencing growthinduced or growth-strengthened oscillations cannot reach a relatively steady state (an equilibrium or relatively small oscillations) within a finite time or reasonable relaxation period.

Growth-Induced Switching Among Coexisting Attractors When coexisting attractors are present in the circuit dynamics, such as bistability or multistability, the circuit typically only functions with one of the attractors. In other words, the circuit is functional locally in its phase space rather than globally. Strengthened growth can push the system across the boundary of different attracting basins in the circuit phase space, causing the circuit to lose its desired functionality by switching from a functional basin to a malfunctioning basin.

Growth-feedback induced oscillations

As demonstrated by the light green and yellow slices of the pie chart in **Fig. 2**, a considerable portion (17%) of the circuit failures are caused by growth-feedback-induced oscillations. Growth feedback perturbations can easily change the system from the adaptive domain to the oscillation domain in these cases. Our program classifies oscillation-mediated failures into two categories: continuous (type-III) and discontinuous failures (type-IV). Type-III failures are the results of either (i) a gradual increase in the oscillation amplitude, or (ii) a gradual increase in the transient lifetime of damped oscillations. In the first case, an isolated circuit has already exhibited oscillations with small amplitudes in its gene concentrations with relatively weak growth feedback. As the feedback is strengthened with a larger value of k_g, the oscillations are intensified with a larger amplitude, leading to a circuit failure. In the second case, there is damped oscillation for small k_g with a relatively short transient time before approaching an equilibrium. After strengthening the growth feedback, the damping weakens and the oscillation's amplitude cannot be reduced to the threshold within the time limit, as exemplified in **Fig. 2(c)**.

The second category of growth-feedback-induced oscillation is type-IV, where oscillations emerge suddenly as the growth-feedback strength increases through a critical point. The sudden emergence of oscillations can be caused by a bifurcation or a transition into a basin of a limit-cycle attractor. A random sampling of the type-IV failure cases reveals that most of them are caused by either a saddle-node bifurcation of cycles (*Strogatz, 2018*) or an infinite-period bifurcation (*Stro-* gatz, 2018). In the former case, a pair of stable and unstable limit cycles suddenly emerge together. In the latter case, when observed from the opposite direction (i.e., with a decreasing k_g crossing the threshold), the oscillation in the system spends a longer and longer time around a node on the limit cycle. This node finally becomes a stable fixed point at the bifurcation point, and the oscillation period approaches infinity. One example of type-IV oscillation-mediated failures caused by an infinite-period bifurcation is shown in **Fig. 2(d)**. In our simulations, most of the

cases where there are saddle-node bifurcations of cycles are categorized as type-III failures because, prior to the bifurcation point, the system can be oscillating near the ghost (*Strogatz, 2018* ⮕) cycle for a long time exceeding the criterion for relaxation time, though that ghost cycle is not an attractor but only a transient in the system.

Our results indicate that for various circuit topologies, the dynamic mechanisms leading to failures can differ, resulting in significantly different distributions of failure types among different networks. For instance, the fractions of failures caused by growth-induced oscillations can vary dramatically among all the topologies, as demonstrated in **Fig. 3(a)** ⮕, where each data point represents a specific network topology. The fraction of failures caused by growth-induced oscillations can range from approximately zero to about 80%! A particular example of two different networks is presented in **Figs. 3(b1)** ⮕ and **3(b2)** ⮕, both of which share the same minimal topology required for adaptation (*Shi et al.*, *2017*) - the circuit's core function. Despite differing by only one link, the proportions of failures with unique mechanisms are quite distinct, as illustrated in **Figs. 3(c1)** ⮕ and **3(c2)** ⮕. Notably, for the network in **Fig. 3** ⮕(b1), almost half of the failures result from oscillations, while hardly any oscillation-mediated failures occur for the network in **Fig. 3(b2)** ⮕. The explanation is that, although the difference lies in only a single link, this link determines whether an oscillation-correlated motif exists within the network. Previously, three classes of motifs capable of supporting persistent oscillations were discussed (*Novák and Tyson, 2008* ⮕), including the "delayed negative-feedback loop" featured in **Fig. 3(b1)** ⮕.

Generally, the circuit dynamics depend sensitively on the structure, but oscillations specifically require a negative feedback loop with time delay (*Novák and Tyson, 2008* ⮕). Since there are no explicit time-delayed terms in the dynamical equations in our model, one of the two types of motifs - an intermediate node in the path of the negative feedback loop or an additional positive feedback loop - is necessary to induce time delay (*Novák and Tyson, 2008* ⮕). For network topologies with a high ratio of functional failures caused by oscillations, both motifs are observed, especially the former type. For the network in **Fig. 3(b1)** ⮕, the three links: A → C, C ⊣ B, and B → A, together constitute a negative feedback loop, making the circuit more susceptible to oscillatory behaviors. For the circuit in **Fig. 3(b2)** ⮕, no such negative feedback loop exists. **Figure 3(a)** ⮕ summarizes the total number of failed trials and the ratio of oscillation-induced failures for each network topology. The network topologies that contain one of the motifs for oscillation as discussed in *Novák and Tyson* (*2008*) are marked in red, while the networks that do not consist of any of them are marked in blue. Note that all the networks with relatively high ratios of oscillation-induced failures (e.g., ratio > 0.2) consist of oscillation-correlated motifs. Details about these oscillation-correlated motifs are discussed in **Appendix 2** ⮕.

We conclude that, for a network with an oscillation-correlated motif, even if it is functional at some parameter values, the potential of oscillatory behaviors can be triggered by growth feedback. As a result, networks without these motifs can be safer choices to avoid too many failures cases due to oscillations. Note that this relationship is not deterministic. As shown in **Fig. 3** ⮕, even the networks represented by blue dots that have no oscillation-correlated motifs can still have oscillation-induced failures (with small ratios). The complexity of the scenario makes it challenging to find general and relatively simple rules that connect circuit topology to the circuit's robustness.

Bistability and bifurcations

In this section, we describe the dynamical mechanisms behind type-V and type-VI failures, which in total take up about 14% of all the circuit failures. These failures are abrupt, meaning that the response curve undergoes an abrupt change at a certain critical value of k_g from a desirable curve of adaptation. Type-V and type-VI failures correspond to an abrupt change in O_1 and O_2, respectively. Both types of failures are closely related to bistability and bifurcations.
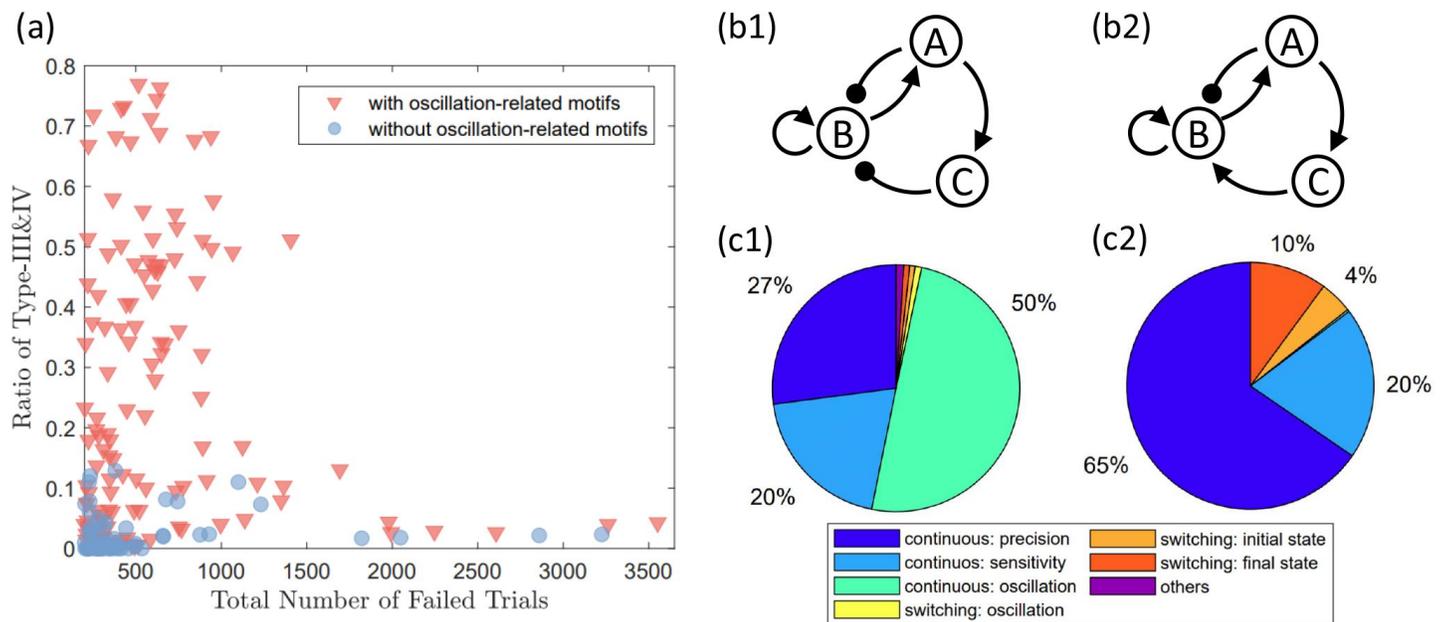
Figure 3.

Frequencies of growth-feedback induced oscillation failures for different network topologies. (a) Significant variations in the proportion of trials resulting in circuit failures due to growth-feedback-induced oscillations (types III and IV failures) across distinct network topologies. Some topologies exhibit virtually no oscillation-related malfunctions, while others experience about 80% of failures caused by growth-induced oscillations. Network topologies containing any oscillation-supporting motifs (discussed in the main text) are represented by red triangles, while the rest are shown as blue circles. The majority of red data points have higher fractions of oscillation-related failures compared to the blue ones, mainly due to the presence of oscillation-supporting motifs. To reduce fluctuations in the results, only circuit topologies with over 200 failed trials are included. (b1, b2) A pair of network topologies that differ by only one link (from node C to node B). (c1, c2) The distinct topologies in (b1, b2) leading to different distributions of failure mechanisms. The topology in (b1) primarily experiences growth-induced oscillation as the major failure mechanism, while the one in (b2) has barely any trials with growth-feedback induced oscillations.

Bistability and multistability are common phenomena in nonlinear systems. Bistability refers to the situations where two stable attractors coexist in the phase space simultaneously. Multistability describes a similar coexisting phenomenon of attractors, but with more than two attractors. With bistability or multistability in the target dynamical system, the system trajectory may end up in any one of these stable attractors, depending on the initial state of the system evolution. The entire phase space can thus be separated into two or more basins of attraction. Each basin of attraction corresponds to an attractor and consists of all the initial states that eventually lead the system to the attractor. The boundary boundaries separate two different basins of attraction. A close pair of initial states but at different sides of a basin boundary lead the system to different attractors.

In our simulations, we observe bistability in many circuits. While multistability has also been observed, it is relatively rare. We thus focus on bistability. It is highly unusual for both attracting basins to exhibit the desired functional behavior simultaneously. This is because they are located in different regions of the system phase space, and accommodating both would impose overly stringent constraints on the circuit. Having one basin functional is already difficult enough with a random sampling of circuit parameters. As a result, functional adaptation is typically found in only one of the basins, with adaptation being lost in the other, and the circuit is functional only locally in its phase space, rather than on a global scale. A drifting system parameter, such as k_g, can alter the dynamics of the gene circuit. In a situation with bistability, such a change in the system dynamics can modify the shape and position of the basin of attraction and the basin boundary. Consider an initial state close to a basin boundary. With the deformation caused by a drifting parameter, the boundary may shift across the initial state, leading to a sudden switching of the system's final attractor. If the basin before the parameter change is functional and the basin after is not, this leads to a growth-feedback-induced failure. The crossing of the basin boundary dictates that the system's final state will abruptly change from one attractor to another. This type of failure can be classified as a switching type of failure.

An example of bistability-related failures is shown in **Fig. 2(e)** ⬚, where in the upper panel, the circuit enters into the functional region after an initial transient. In the lower panel, the circuit enters into another region that does not have adaptability, and the circuit does not respond to the switching of the input signal. **Figures 4(a)** ⬚ and **4(b)** ⬚ illustrate how the basin structure of the circuit changes significantly with different values of k_g. The functional basin is in yellow and it shrinks greatly with an increasing k_g. Note that the phase space is four-dimensional, so only a two-dimensional slice is shown. For a bistability/multistability-induced type-V failure where O_1 is switched, the boundary of the functional basin crosses the initial state. For a type-VI failure, the simultaneous movement of both O_1 and the basin boundary under input I_2 results in O_1 crossing the boundary.

Bifurcations also play an important role in many type-V and type-VI failures. An example of a failure caused by a fold bifurcation is shown in **Fig. 2(f)** ⬚ and the corresponding bifurcation diagram is shown in **Fig. 4(c)** ⬚, where a non-functional fixed point appears through a fold bifurcation as k_g crosses a critical value. Bifurcation-induced abrupt failures differ from those caused by bistability/multistability, but they can be related since significant changes in the basin structures often occur near a bifurcation point.

Circuit robustness and optimal topology

To quantify a circuit's robustness against growth feedback, we introduce two metrics: Q-value and R-value. We track the number of remaining functional trials for each network for various k_g values (starting from $k_g = 0$), denoted as $Q(k_g)$. This measure extends the concept of Q-values in **Ma et al. (2009** ⬚) by accommodating non-zero values of k_g. To characterize the circuit robustness, we define the survival ratio $R(k_g)$ as $R(k_g = k) = Q(k_g = k)/Q(k_g = 0)$. This ratio represents the fraction of random circuit realizations that maintain functionality under growth feedback with a strength of k_g.
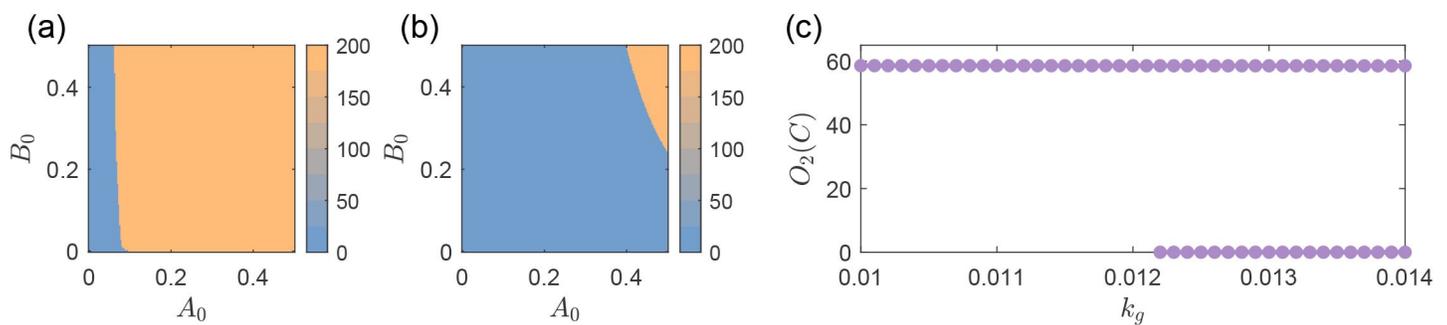
Figure 4.

Two possible mechanisms behind both the type-V and type-VI failures. (a,b) Basin structure of the circuit shown in **Fig. 2(e)** ⧉ (with type-V failure) for input I_1 with different levels of growth feedback, for growth feedback strength $k_g = 0.05$ (weak) and $k_g = 0.97$ (relatively strong). The coordinates A_0 and B_0 are the initial values of nodes A and B, respectively, corresponding to a two-dimensional slice of the entire four-dimensional phase space by fixing $C = 0.1$ and $N = 10^{-3}$. The color bar indicates the equilibrium value of node C before the input switch, which is $O_1(C)$. There is bistability in both cases, as there are two basins of attraction. The yellow region is the functional basin that has adaptation, while the blue region is a non-functional basin without adaptation. The relative size of the blue non-functional region with larger k_g in this case is significantly larger and includes the initial state of the system ($A_0 = B_0 = 0.1$), causing a type-V circuit failure. (c) Bifurcation diagram of the circuit in **Fig. 2(f)** ⧉ with a type-VI failure. Prior to a critical value of $k_g \approx 0.0122$, only one stable value of $O_2(C)$ exists. There is a fold bifurcation at the critical value, giving birth to a new state around zero, which is non-functional. For an abrupt failure, whether it belongs to type-V or type-VI does not determine whether it is caused by bistability or bifurcations. Both mechanisms are possible for both types of failures.

Note that each $Q(k_g)$ or $R(k_g)$ is defined for a specific network topology in a suitable parameter space. A high value of $R(k_g)$ indicates that a large fraction of the randomly sampled circuit parameters is functional despite cell growth with any strength no larger than k_g, indicating that the topology is more robust against growth feedback. Because of the detrimental effects of growth feedback, $R(k_g)$ decreases monotonically with respect to k_g.

To justify the utility of $R(k_g)$, we test the circuit topologies employed in a previous work (***Zhang et al., 2020***), where two relatively simple network topologies were used for a comparison study in terms of their ability to resist growth feedback and remain functional. Our evaluation of $R(k_g)$ for the two topologies has yielded results that are consistent with those in ***Zhang et al.*** (***2020***), as discussed in Appendix 3 . To illustrate our results in a concrete way, we set $k_g = 0.6$ and calculate the ratio $R(k_g = 0.6)$ for different network topologies.

Our computations have revealed a set of eight circuit topologies with optimal performance as characterized by high values of both $Q(k_g = 0)$ and $R(k_g)$, as indicated by the set of orange points in **Fig. 5(a)** . The optimal circuits form a family as their topologies exhibit a high level of similarity with one other. In particular, all eight circuits in this family share a common set of links (motif), as shown in **Fig. 5(b)** . The combination of these common links is one of the minimal topologies with perfect adaptation in a three regulatory logic (***Shi et al., 2017***) and is critical for the circuit to be functionally adaptable. The only difference among the circuits in this family is the links from node C. While an inhibition link from node C can be important to achieving a value of $R(k_g)$, as discussed below, the eight optimal circuit topologies do not contain any such inhibition link from node C. (The role of this particular link will be further studied in our analysis of the results in **Fig. 6** .) This also explains why the family has eight members, as follows. Each link from C has two options: either the link does not appear, or it appears as an activation link. As there are three possible links from C (C to A, C to B, and C to C), there are altogether eight (2^3) topologies within this optimal family, according to the simulation results in **Fig. 5** .

How can we quickly determine if a three-gene regulatory network with a given topology can be robust against growth feedback? Is there any structural feature of the circuit that can be used to estimate if a high value of $R(k_g)$ can be achieved? To gain insights, we observe that the histogram in **Fig. 6(b)** has three peaks about low, moderate, and relatively high values of R, respectively. Computations reveal certain "shared topological similarity" (or motif) within each peak. Thus, each peak corresponds to a group of similar network topologies that simultaneously have a similar level of R. This observation suggests a correlation between the network topology and robustness against growth feedback. For convenience, we refer to these three groups of networks by the colors presented in **Fig. 6** . For instance, the group with the highest R (the green triangles in **Fig. 6(a)(d)**) is called the green group, and the group with the lowest R (the red diamonds in **Fig. 6(a)(d)**) is the red group.

To better distinguish the three groups, we introduce two binary variables, B_1 and B_2. For each network, $B_1 = 1$ if the network contains the motif in **Fig. 6(c)** , and $B_1 = 0$ otherwise. Then, for each network, an additional binary variable is set to be $B_2 = 1$ if there is an inhibition link from the output node C, and $B_2 = 0$ otherwise. We find that a linear combination of the two binary variables, $B_S = B_1 - B_2$, can characterize the circuit topology and robustness against growth feedback. In particular, the three possible cases $B_S = 0$, 1, or -1 correspond to the three peaks in **Fig. 6(b)** . This result suggests that the motif shown in **Fig. 6(c)** is beneficial for robustness, while an inhibition link from the output node C is detrimental. It is the balancing act of these two factors that determines the overall circuit robustness.

The discovery of this three-peak structure and the corresponding topological similarity within each peak is facilitated with the use of machine learning. In particular, we consider a simple type of artificial neural network called multilayer perceptron (MLP), where we train it to predict the R value from the input of the network topology through a small hidden layer with only two nodes, as
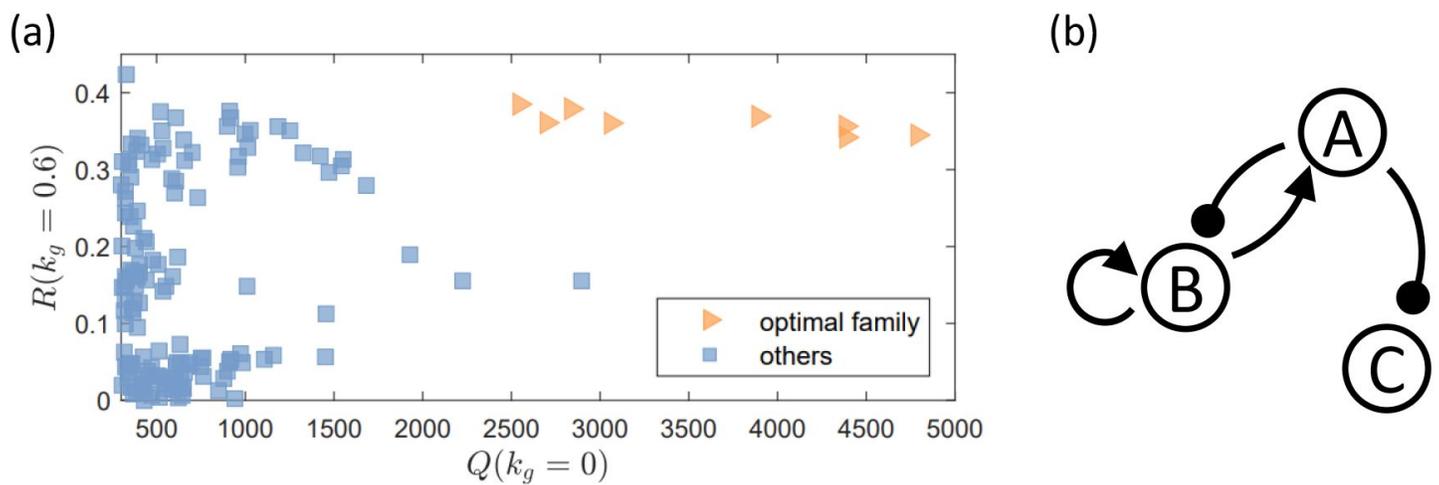
Figure 5.

A family of circuit topologies with optimal performance. The circuits both have a large volume of the functional region in the parameter space in the absence of growth feedback as characterized by a large value of $Q(k_g = 0)$ and are robust against growth feedback with a high value of $R(k_g)$. (a) Values of $Q(k_g = 0)$ and $R(k_g = 0.6)$ from all the 425 network topologies, where each data point corresponds to a topology. The family of optimal topologies is represented by the orange data points, including eight network topologies. (b) The set of links (motif) shared by this family of circuits. The combination of these links is also one of the minimal topologies with perfect adaptation in three regulatory logic (***Shi et al., 2017*** 🗗).
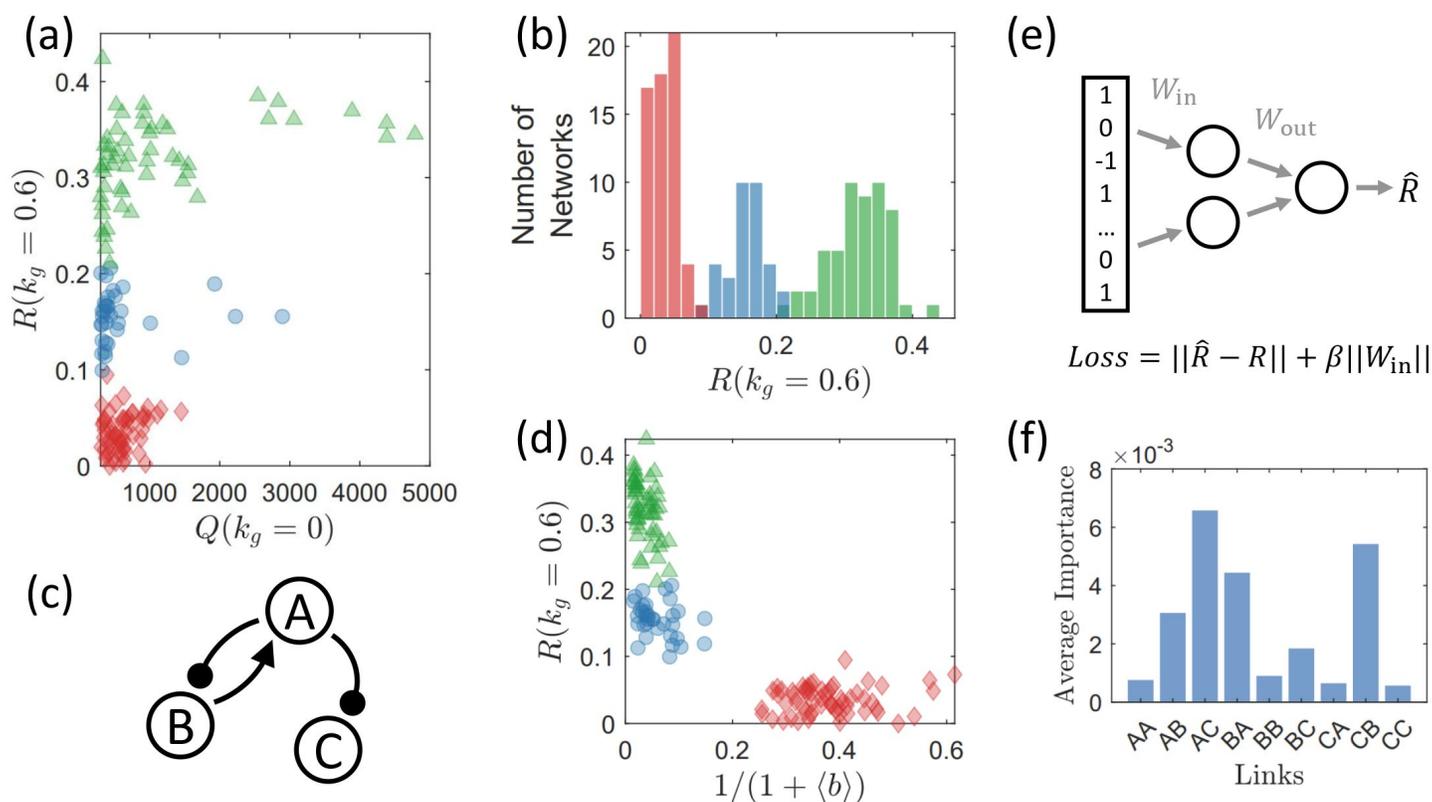
Figure 6.

Strong correlation between circuit robustness against growth feedback and circuit topology. There are three groups of circuits, each displaying strong topological similarities within, exhibit distinct levels of robustness against growth feedback as measured by the characterizing quantity R. (a) Robustness measure $R(k_g = 0.6)$ versus $Q(k_g = 0)$ for all 425 network topologies. Circuits are color/shape-coded into three groups (green triangles, blue circles, and red diamonds) based on the rules defined in the text. The three groups of topologies display distinct levels of $R(k_g = 0.6)$ values, signifying a strong correlation between circuit robustness and topology. Only circuits with $Q(k_g = 0) > 300$ are shown to reduce fluctuations arising from random parameter sampling. What is demonstrated is the case of an intermediate level of growth feedback with $k_g = 0.6$ (a different value of k_g has no significant effect on the results - see **Fig. 7** ☐). The topologies associated with the green triangles have a high level of robustness, which can be regarded as an optimal group and is more prevalent than the optimal group identified in **Fig. 5.** **(b)** ☐ Histogram of $R(k_g = 0.6)$ the same color legends as in (a). Three distinct peaks emerge, each associated with a group of circuit topologies. (c) The shared network motif among all networks in the green group, which is highly correlated with the optimal minimal network shown in **Fig. 5(b)** ☐, but without the link B → B, which is necessary for the NFBL family of networks to have adaptation (**Shi et al., 2017** ☐). (d) Effects of burden b for the three groups of networks, where the abscissa is the effective term of burden in the formula of growth rate Eq. (12) ☐. The circuits in the red group have larger values of $1/(1 + \langle b \rangle)$, suggesting that a heavier burden yields a stronger effect of the growth feedback for the red group. (e) A multilayer perceptron (MLP) for identifying the crucial connections that determine the robustness of the circuits. The circuit topology serves as the input, where 1, 0, and -1 represent activation, null, and inhibition links, respectively. The output is a predicted robustness measure, denoted as $\hat{R}$. To encourage the neural network to select as few links as possible for predicting $\hat{R}$, a *l*-1 regularization term, $\beta||W_{in}||$, is incorporated into the loss function alongside the fidelity error $||\hat{R} - R||$. As a result, the feed-forward process eliminates information about the links that have little impact on circuit robustness since the corresponding W_{in} entries automatically optimize to values close to zero. (f) Results from an ensemble of 50 MLPs, each trained with distinct initial values. Shown is the average importance of each of the nine links, which is determined by the weights in W_{in} - see Appendix 4 ☐. The top four links with the highest importance correspond to the four links used to classify the three peaks in panel (b).

demonstrated in **Fig. 6(e)** ⧉ . This bottleneck structure in the hidden layer plus the l-1 regularization imposed on the input matrix W_{in} forces the MLP to extract low-dimensional features from the input topology to estimate R. In our tests, the MLP designed this way automatically assigns different levels of weights to the input information of different links. Over an ensemble of 50 MLPs trained with different random initial values, the ranking of average importance is shown in **Fig. 6 (f)** ⧉ . The top four links are the four links used to categorize the three peaks.

The results in **Fig. 6** ⧉ is for k_g = 0.6. However, we find that different values of k_g lead to essentially the same ranking of $R(k_g)$ among the circuit topologies, as illustrated in **Fig. 7** ⧉ .

Three remarks on our categorizing rules based on the two extracted featured motifs are in order.

First, the shared motif for the green group is strikingly similar to the optimal minimal network in **Fig.5(b)** ⧉ (the orange group). The sole distinction lies in the self-activation link of node B. This specific link plays a crucial role. Every network in the NFBL family depends on this link to achieve adaptation (***Shi et al., 2017***). However, for circuits within the IFFL family, this link is not a necessity for adaptivity. Missing this link makes the motif in **Fig. 6(c)** ⧉ no longer a minimal network for adaptation, and a circuit containing this motif may either belong to the NFBL or the IFFL family. We have thus identified two optimal groups: the green group with optimal robustness R and the orange group with both the optimal robustness R and the largest functional volume $Q(k_g$ = 0) in the absence of growth feedback. The orange group is a subset of the green group, with an additional requirement for $Q(k_g$ = 0).

Second, the shared motif for the red group is also exactly the group of all circuits containing an inhibition link from node C to node B, denoted as C ⊣ B. These two different definitions are in fact equivalent: all networks with $Q(k_g$ = 0) > 300 that contain C ⊣ A or C ⊣ C also contain the motif in **Fig. 6(c)** ⧉ , yielding B_S = 0, and belong to the blue group.

Third, the three circuit groups in **Fig. 6** ⧉ are not correlated with the categories used in previous research on circuit functionalities without growth feedback (***Ma et al., 2009*** ⧉ ; ***Shi et al., 2017*** ⧉). These studies classified adaptive networks into NFBL and IFFL families. Each family contains a few minimal topologies with or without some additional other motifs, and the two families have distinct minimal functional topologies. The minimal topology acts as the backbone for supporting circuit functionality. We find that, when growth feedback is present, the prior classification scheme and the underlying minimal topologies become less relevant. Circuits belonging to the NFBL family are spread across all three levels of $R(k_g)$ in **Fig. 6(b)** ⧉ , as are the circuits from the IFFL family. A robust circuit can be part of either family, just as a fragile circuit can belong to both. We give that: (i) the topological motifs determining circuit functionality robustness and (ii) the motifs deciding whether a circuit belongs to the NFBL or IFFL family are independent. To quantify this irrelevance, we calculate the point biserial correlation between $R(k_g$ = 0.6) and a binary variable determining the family to which the circuit belongs. The resulting correlation is merely 0.1, suggesting hardly any correlations. A further illustration and quantification of this irrelevance can be found in **Appendix 5** ⧉ .

What are the reason and mechanism behind the phenomenological set of circuit categories? Especially, it is desired to understand why the shared motif for the green group is beneficial for circuit robustness, and why the shared motif for the red group is harmful for robustness. It is challenging to find straightforward explanations given the complexity of the problem (see Discussion section). Certain insights are as follows. We find that the average node concentrations at the equilibrium for the network topologies in the red group are consistently smaller than those in the blue group. This difference is reflected in the value of burdens b. In particular, according to **Eq. (12)** ⧉ , the cell growth rate is proportional to the term $1/(1 + \langle b \rangle)$ under the same level of growth feedback. **Figure 6(d)** ⧉ shows the average burden b for each network topology,
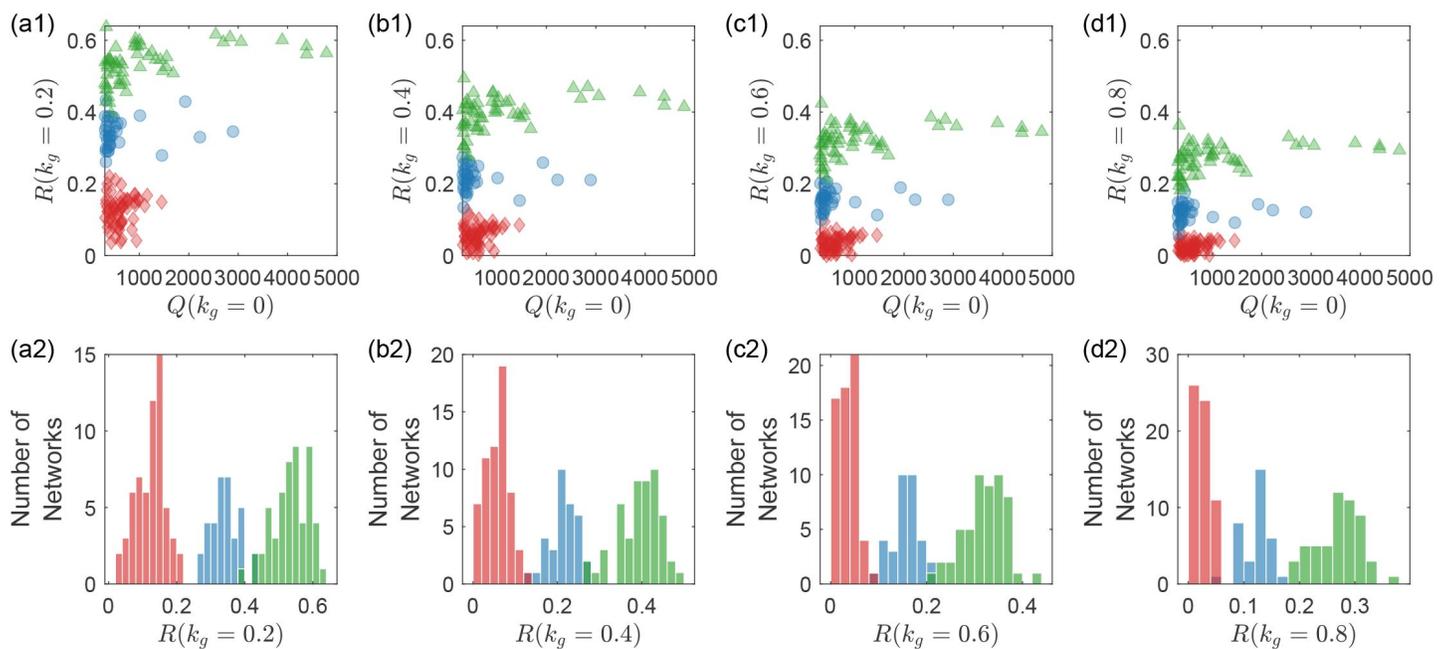
Figure 7.

Robustness of the circuit division into three groups subject to different levels of growth feedback. From the top to the bottom, the four rows are for k_g = 0.2, k_g = 0.4, k_g = 0.6, and k_g = 0.8, respectively. The legends are the same as in **Figs. 6(a)** ⧉ and **6(b)** ⧉. For different levels of growth feedback, the distribution of the robustness measure exhibits three distinct peaks that occur at approximately the same locations on the R axis. The implication is that the division of the circuit topologies into three groups in terms of the robustness measure can be revealed by examining the circuit functions at a single value of the growth feedback strength.

demonstrating that the values of the term $1/(1 + \langle b \rangle)$ for the circuits in the red group are larger than the values in the blue group. As a result, for the same value of k_g, the growth feedback effectively received by the circuits in the red group is stronger than that of the blue group circuits. Further support is provided by the results from the limit $J \to \infty$ (**Appendix 6** ⬀). In this limit, the burden b does not affect the strength of the growth feedback. As a result, the R values of the red group significantly overlap with those of the blue group, suggesting that the distinctively low values of R for the red group be a result of the burden with finite J. We also find that the existence of the shared motif for the red group has a stronger correlation to the motif necessary for growth-feedback induced oscillations. All circuits with oscillation type of failures taking up more than 20% of failures belong to the red group. This correlation can result in further fragility of the red group circuits.

Scaling law quantifying the effect of growth feedback on gene circuits

A comprehensive way to understand the effects of growth feedback on gene circuits is through scaling laws, an approach commonly employed in statistical and nonlinear physics. Does a scaling law exist that characterizes quantitatively how growth feedback affects the circuit functioning? Through a systematic computational analysis of the circuit robustness, we have uncovered a scaling law that governs how the robustness measure $R(k_g)$ deteriorates as growth feedback is strengthened, as shown in **Fig. 8** ⬀, where the blue curve is the result averaging over all the 425 network topologies. The three other curves represent circuits that have a relatively high, moderate, and low value R among the 425 topologies tested. As growth feedback is strengthened, the number of circuit topologies that can maintain functioning decreases (or, equivalently, the number of failed circuits increases). The decreasing behavior of $R(k_g)$ with k_g tends to be slower than exponential [e.g., $\exp(-\beta k_g)$ with $\beta > 0$ being a constant].

A general theoretical argument for the scaling law is unavailable. However, if we simplify the system by setting the parameter J in **Eq. (12)** ⬀ to be large so the burden $b(t)$ is much smaller than one, we are able to argue that the scaling law is approximately given by

$$R(k_g) \sim \exp(-\beta k_g^\lambda), \qquad (1)$$

where $\beta > 0$ and $0 < \lambda < 1$ are two specific constants that depend on the network topology, and the typical value of λ is about 0.6. The exponential scaling is assumed, given its memorylessness. That is, there is no special zero point of k_g, for the reason that a certain level of k_g is mathematically equivalent to a larger d_x, as discussed below.
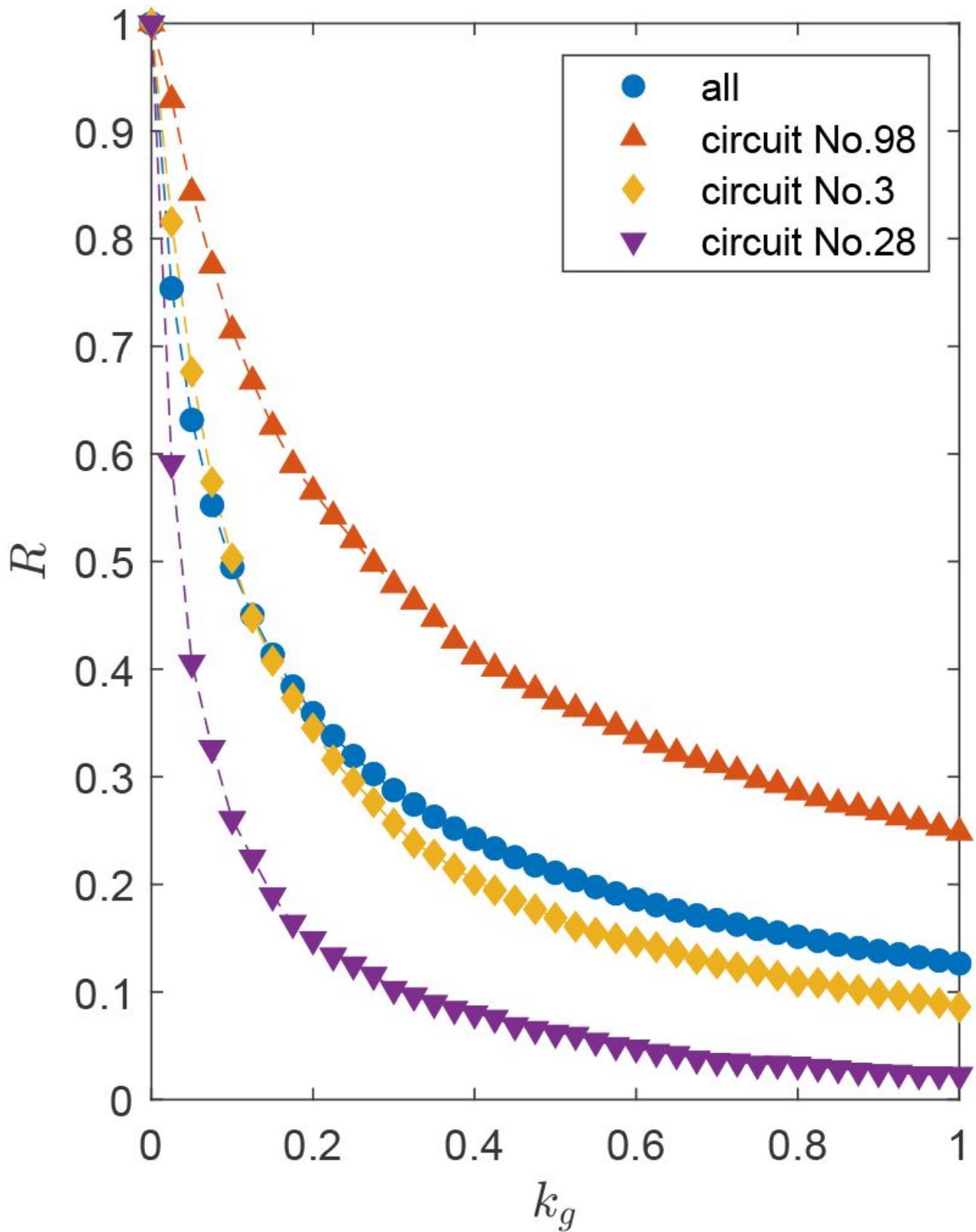
Figure 8.

Scaling law governing the circuit robustness measure $R(k_g)$. The blue curve is the average result of all the 425 network topologies. The other three curves are from three types of circuits with relatively high, moderate, and low values of R among the 425 circuit topologies tested.

The quantity $R(k_g)$ is a simple and straight-forward measure characterizing the detrimental effect of growth feedback on gene circuits. We carry out a semi-quantitative analysis of this quantity and the effect of k_g on it. The circuit dynamical equations **Eqs. (9 ☑-12 ☑)** can be simplified by substituting **Eq. (14) ☑** into them to cancel the dN/dt terms, leading to

$$\frac{dA}{dt} = v_A \frac{I^{n_{IA}}}{I^{n_{IA}} + K_{IA}^{n_{IA}}} - (d_A + k_g \frac{1}{1+b})A, \quad (2)$$

$$\frac{dB}{dt} = v_B \frac{A^{n_{AB}}}{A^{n_{AB}} + K_{AB}^{n_{AB}}} - (d_B + k_g \frac{1}{1+b})B, \quad (3)$$

$$\frac{dC}{dt} = v_C \frac{A^{n_{AC}}}{A^{n_{AC}} + K_{AC}^{n_{AC}}} \frac{K_{BC}^{n_{BC}}}{B^{n_{BC}} + K_{BC}^{n_{BC}}}$$
$$- (d_C + k_g \frac{1}{1+b})C. \quad (4)$$

Compared with the equations without growth feedback **Eqs. (6 ☑ -8) ☑** , we see that introducing growth feedback is equivalent to adding a variable $k_g/(1 + b)$ to the degradation terms for each node. Intuitively, the value Q of a network topology measures the volume of the functional region $\mathcal{M}$ in the parameter space, which is also a function of k_g. We thus have that $R(k_g = k)$ is the volume of the intersection between $\mathcal{M}(k_g = k)$ and $\mathcal{M}(k_g = 0)$ divided by the volume of $\mathcal{M}(k_g = 0)$:

$$R(k_g = k)$$
$$= V(\mathcal{M}(k_g = k) \cap \mathcal{M}(k_g = 0))/V(\mathcal{M}(k_g = 0)), \quad (5)$$

where $V(\mathcal{M})$ is the volume of $\mathcal{M}$.

The picture can be further simplified if we assume the burden b is approximately a constant within a range of k_g. Since growth feedback contributes to an additional term in degradation d_x, strengthening the feedback is equivalent to increasing all three quantities d_x together. Consequently, as k_g increases, the high dimensional region M does not deform, but simply translates in the negative direction in all dimensions of degradation d_x in the parameter space. That is, as growth feedback becomes stronger, it becomes more difficult for the circuit to maintain it functioning.

Discussion

When a synthetic gene circuit is introduced into a host cell, an inherent coupling arises wherein the gene circuit affects cell growth and cell growth in turn alters the circuit gene expression (***Klumpp et al., 2009 ☑***; ***Klumpp and Hwa, 2014 ☑***). Due to the fundamental nonlinearity in the gene network and in the cell growth dynamics, the interaction is generally quite complicated. To understand this interaction so as to identify the circuit topologies that can withstand the interaction and maintaining the intended circuit functions is one of the most challenging problems in synthetic biology.

Previous studies showed that growth-mediated feedback can endow synthetic gene circuits with various emergent properties. In general, growth feedback tends to negatively impact the intended function the circuit is designed for. There was preliminary evidence that the effects of growth feedback depend strongly on the circuit topology (*Zhang et al., 2020*). For a particular circuit function, while the vast majority of the topologies would fall under growth feedback, a handful still exists that is adaptable to maintain its designed functions. Identifying the "optimal" topologies that are most robust against growth feedback is fundamental to constructing synthetic gene circuits that can survive, adapt, and function as designed in the fluctuating growth environment of the host cells.

The main contribution of this paper is a systematic computational study of three-gene circuits with adaptation to uncover and understand the detrimental effects of growth feedback on gene circuits and to identify optimal groups of topologies. Without growth feedback, there are 425 possible topologies with functional adaptation. A vast majority of these circuit topologies fail in their functions under growth feedback, and our computations have revealed, for the first time, six distinct main failure categories covering more than 99% of the cases. From a dynamical point of view, there are three mechanisms by which growth feedback can deprive the circuit of its ability to adapt: (i) continuous deformation of the response curve, (ii) strengthened or induced oscillations, and (iii) sudden switching to coexisting attractors (also summarized in *Box 1*). By introducing a robustness measure to quantify circuit adaptation in the presence of growth feedback, we uncover a general scaling law characterizing the detrimental effect of growth feedback on the circuit functioning in a quantitative manner. We identify an optimal group of circuits with high robustness and key subsets of links associated with this group that play a critical role in sustaining circuit function in host cells. Taken together, to design a functional gene circuit, growth feedback must be taken into account, as the same circuit designed with perfect functions without the feedback can behave quite differently when the feedback is present. Our study has provided unprecedentedly quantitative insights into the interplay between gene circuit topology and growth feedback, unlocking the dynamical mechanism of growth-induced failures and providing guidance to better design practically applicable synthetic gene circuits.

A unique finding is that growth feedback can induce or strengthen oscillations in gene circuits designed for adaptation. Such oscillations can often destroy the circuit functionality. In a recent experimental study, a similar phenomenon was observed in gene circuits designed for self-activation (*Melendez-Alvarez et al., 2021*). These results suggest that growth-feedback induced oscillation may be a general dynamical mechanism that can negatively affect the robustness of gene circuits. In addition, our study has shown that growth feedback has a highly sensitive dependence on the circuit topology: even a small structural differences between two circuits designed for the same function can result in drastically different outcomes under growth feedback. For example, **Fig. 3** demonstrates that a link critical for an oscillation-supporting motif can significantly affect the robustness of the circuit against growth feedback. It can thus be quite useful to identify failure-related motifs so that they can be avoided when designing a gene circuit.

From a broad point of view, our study has yielded basic insights into the fundamental topology-function relationships in gene circuits. Examples include how circuit topology affects circuit robust-ness against growth feedback and whether a circuit topology contains motifs supporting a specific type of growth-induced failure, such as oscillation-related malfunctions. However, searching for and understanding the interplay between circuit topology and dynamical behaviors remain to be a challenge, for the following five reasons.

First, the two relevant questions are whether a circuit topology supports adaptation and whether the circuit is robust against growth feedback or is susceptible to a specific type of growth-induced failures. While our study focused on the latter, the former is important. Addressing both questions to identify and analyze all possible scenarios is infeasible at the present, due to the complex

parameter space of the circuits. To make our study feasible, we focused on the cases where the circuit satisfies all the requirements for adaptation in the absence of growth feedback. These cases may occupy a small region in the entire parameter space of the circuit. For each circuit topology, the uncovered function failures due to growth feedback are thus limited to relatively small parameter regions. Second, most network topologies studied have dense connections among the three nodes (only about 20% of the networks have fewer than six connections). As a result, different motifs can overlap with each other, blocking or enhancing the function of each other. The dense connections thus pose a difficulty in identifying the motifs accurately. Third, for a particular class of failures, competition among different failure types may arise. For instance, a circuit with oscillation-supporting motifs may not have a high fraction of oscillation-induced failures because it also contains the motif for bistability, leading to a large fraction of failures due to the bistability-induced malfunctions. Fourth, due to the necessity to set a threshold in the relaxation time, transient behaviors can arise. In many failure cases caused by oscillations, the oscillatory behavior is not stable and the circuit will eventually approach a fixed point. However, time scales should be taken into account. The transient behaviors can make the network topologies without the necessary motif for sustained oscillations exhibit oscillation-induced failures. Fifth, growth feedback acts as additional feedback loops within the circuit, potentially complicating the circuit dynamics and adding more links to the circuit topology. These extra links in the integrated topology might give rise to an oscillation-related motif. However, our simulations have shown that the impact of this additional oscillation motif, introduced by growth feedback, tends to be weak (**Appendix 6**).

In **Appendix 7**, we extend our analysis to four-gene circuits with over two thousand functional failure trials. A remarkable finding is that the failure scenarios for these four-gene circuits are the same as the categories for three-gene circuits (summarized in **Box 1**), indicating that the growth-feedback induced failure mechanisms identified in our work are general.

The primary goal of this paper is to explore the ways in which growth feedback can undermine a gene circuit's functionality, and we have uncovered three main dynamical failure mechanisms. The reason that we focus on small gene circuits (i.e., those with three or four genes) is that, in current synthetic biology, only small gene circuits are of interest. The main reason is that, even for a modest number of genes, when the circuit is introduced to a host, the competition and interactions in the form of growth feedback are likely to lead to unintended and uncontrollable consequences. Another reason is resource competition: the genes in the circuit could compete for the limited resources in the host cell, negatively impacting the circuit dynamics. Because of the two reasons, at present large gene circuits are not favored in synthetic biology. In fact, the state-of-the-art synthetic gene circuitry usually involves three or four genes, where the consequences of growth feedback had been poorly understood. Our work fills in this knowledge gap.

It is possible that, in the future, synthetic biology may use larger and more complex circuits. To uncover and understand the failure mechanisms as well as to identify circuits that are resilient to growth feedback, machine learning can be used. For example, recurrent neural networks have recently been used to identify circuit topologies appropriate for a specified desired function (*Shen et al., 2021*), and reinforcement learning tackle the combinatorial optimization problem (*Bello et al., 2016*; *Mazyavkina et al., 2021*) of pinpointing the optimal circuit topologies. Furthermore, automated differentiation (*Hiscock, 2019*; *Kong, 2022*) can be exploited to locate optimal network parameters, which can be efficient for larger circuits with a high-dimensional parameter space. In spite of these works, to study the effects of growth feedback and resource competition among numerous genes in larger circuits remains to be a formidable challenge. Our work providing a comprehensive picture of the failure mechanisms induced by growth feedback represents a step forward in this field.

Models and Methods

Model description

We restrict our study of the class of transcriptional regulatory networks (TRNs) with the AND logic. For an isolated circuit (in the absence of any growth feedback) with the topology specified inside the red dashed box in **Fig. 1(a)** 🔗, the dynamical equations are

$$\frac{dA}{dt} = v_A \frac{I^{n_{IA}}}{I^{n_{IA}} + K_{IA}^{n_{IA}}} \frac{K_{BA}^{n_{BA}}}{B^{n_{BA}} + K_{BA}^{n_{BA}}} - d_A A, \tag{6}$$

$$\frac{dB}{dt} = v_B \frac{A^{n_{AB}}}{A^{n_{AB}} + K_{AB}^{n_{AB}}} - d_B B, \tag{7}$$

$$\frac{dC}{dt} = v_C \frac{A^{n_{AC}}}{A^{n_{AC}} + K_{AC}^{n_{AC}}} \frac{B^{n_{BC}}}{B^{n_{BC}} + K_{BC}^{n_{BC}}} - d_C C, \tag{8}$$

where the dynamical variables A, B, and C are the concentrations of each protein (node). The notations are as follows. Let x and y be two arbitrary nodes. The quantity v_x is the maximal production rate of gene x, d_x is the degradation rate of gene x, dx/dt is its time derivative of the concentration, n_{xy} and K_{xy} are the coefficients in the Hill function for a transcriptional regulation from gene x to gene y.

When growth-mediated feedback is present, the dynamical equations of the three-node circuits are modified to

$$\frac{dA}{dt} = v_A \frac{I^{n_{IA}}}{I^{n_{IA}} + K_{IA}^{n_{IA}}} \frac{K_{BA}^{n_{BA}}}{B^{n_{BA}} + K_{BA}^{n_{BA}}} - d_A A,$$
$$- \frac{dN}{dt}\frac{1}{N}A \tag{9}$$

$$\frac{dB}{dt} = v_B \frac{A^{n_{AB}}}{A^{n_{AB}} + K_{AB}^{n_{AB}}} - d_B B - \frac{dN}{dt}\frac{1}{N}B, \tag{10}$$

$$\frac{dC}{dt} = v_C \frac{A^{n_{AC}}}{A^{n_{AC}} + K_{AC}^{n_{AC}}} \frac{B^{n_{BC}}}{B^{n_{BC}} + K_{BC}^{n_{BC}}} - d_C C$$
$$- \frac{dN}{dt}\frac{1}{N}C, \tag{11}$$

$$\frac{dN}{dt} = k_g \frac{1}{1 + b(t)}(1 - \frac{N}{N_0})N, \tag{12}$$

$$b(t) = \frac{A + B + C}{J}, \tag{13}$$

where the additional dynamical variable N denotes the density of the host cells, k_g is a parameter controlling the maximal growth rate of the host cells, J is a parameter reflecting how this three-node gene circuit contributes to the burden.

The growth of N is under the regulatory action of two sources: by itself following the logistic equation with the environmental capacity N_0 and by the burden b that represents the competence from the metabolism of the gene circuit. To make the computations feasible, we focus our analysis on the exponential growth phase so that $N_0 \gg N$. The equation governing the growth of the cell numbers, **Eq. (12)** ⬈, can then be rewritten as

$$\frac{dN}{dt} = k_g \frac{1}{1 + b(t)} N, \tag{14}$$

where the dilution rate dN/dt is regulated only by the burden $b(t)$ of the gene circuit. While cell growth is inhibited by the metabolism of the gene circuit, the circuit is also regulated by the growth of N that dilutes the concentration of circuit nodes with increasing cell volume. This dilution is reflected by the additional terms $-(x/N)(dN/dt)$ in **Eqs. (9** ⬈**-11** ⬈**)**.

It is useful to clarify the meaning of the degradation parameter d_x and its relationship to growth feedback. While degradation and growth feedback terms have the same sign in the regulatory equations, d_x may include a constant dilution. We assume that d_x represents the sum of all the degradation effects in cells that are distinct from growth feedback. For instance, degradation tags, especially in the *ssrA* tagging systems (***Gottesman et al., 1998*** ⬈), are often used in synthetic gene circuits to increase the degradation rate and thus increase the time scale of the whole system (***Elowitz*** and Leibler, 2000; ***Fung et al., 2005*** ⬈; ***Stricker et al., 2008*** ⬈; ***O'Brien et al., 2012*** ⬈).

Numerical criteria for functional adaptation

We introduce four criteria to determine if a circuit has functional adaptation.

Precision

The basic requirement of adaptation is that the output remains the same when is input is switched from one state to another, i.e., O_2 should be close to O_1 in Fig. 19b). Specifically, we set the precision criterion to be $|(O_2 - O_1)/O_1| < 0.1$.

Sensitivity

The circuit is also required to respond to the switch of the input signal with a high peak. This ability of the circuit is named sensitivity. We introduce two types of sensitivity: relative and absolute, with the respective criteria $O_{peak}/O_1 > 0.5$ and $O_{peak} > 0.1$. Only the circuits meeting both criteria are regarded as having achieved the required sensitivity.

The need to use the two different criteria simultaneously can be justified, as follows. Given the variety of network topologies and a large number of system parameters, there is a vast diversity in the circuit dynamics and the values of O_1. When O_1 is small, it is difficult to observe a peak that has even satisfied the relative sensitivity criterion. If the absolute criterion is used alone for a circuit with a large O_1 value, the peak may be negligible in comparison with O_1, making its observation practically difficult. It is thus necessary to combine the two criteria so that the cases of small and large values of O_1 can be dealt with on the same footing.

Oscillations

To achieve the desired adaptation, the circuit's output should reach a steady state before and after the input signal is switched. The values of O_1 and O_2 can be determined as the output signal associated with the steady states. However, realistically, it is not necessary to require that the circuit reach an exact equilibrium. Relatively small oscillations in the circuit are acceptable. We define a "relative steady state" where, within a time block of $t_{block} = 200$, the standard deviation of the time series of each node $x(t)$ satisfies: $\text{std}(x) < 1 \times 10^{-4}$ and $\text{std}(x)/\text{mean}(x) < 0.05$. To further

guarantee that the circuit is actually in the "relatively steady state," two successive time blocks satisfying the standard deviation requirements are needed. The quantities O_1 or O_2 are then defined as the respective mean values of the output signal in that last time block t_{block}.

Relaxation time

An ideal gene circuit should be able to respond and adapt within a reasonable time scale. We set an upper bound of evolution time $t_{max} = 4,000$. If the system cannot reach the "relative steady state" within this time, it is regarded as non-functional.

Details of parameter space sampling and response simulation

A three-node gene circuit subject to growth feedback has a large number of parameters. Let L be the number of links among the three nodes (excluding the input link). The total number of parameters is $2 \cdot 3 + 2(L+1) = (2L+8)$. The values of these parameters determine the properties of the regulation links within the circuit and, as a result, the circuit dynamics. The circuit parameters are randomly generated by the Latin hypercube sampling method (*Iman et al., 1980* ☑) using the function "lhsdesign" in Matlab. The parameters are sampled uniformly either on a logarithmic or a linear scale. The sampling ranges of the parameters are: $v_x \in [10^{-1}, 10^1]$ (sampled in logarithmic scale), $d_x \in [10^{-2}, 1]$ (sampled in logarithmic scale), $n_{xy} \in [1, 4]$ (sampled in linear scale), and $K_{xy} \in [10^{-3}, 1]$ (sampled in logarithmic scale).

The dynamical equations of the circuits are numerically integrated by the 4th order Runge–Kutta method with a time step $\Delta t = 0.05$. All the initial states of A, B, and C are taken to be 0.1. The input signal is initially $I_0 = 0.06$ and then switched to $I_1 = 0.6$.

We also observe that, when an isolated circuit fails, a certain amount of growth feedback can restore the circuit's functions. This phenomenon was previously discovered experimentally (*Tan et al., 2009* ☑). However, such cases are rare. We thus focus on circuits that are functional in isolation and examine how growth feedback affects their adaptation.

Acknowledgements

Additional information

Data availability

All relevant data are available from the authors upon request.

Code availability

All computer codes can be found at: *github.com/lw-kong/Growth_Feedback_Adaptation (http://github.com/lw-kong/Growth_Feedback_Adaptation)* ☑

Author contributions

Appendix 1

An Analysis on the Mathematical Criterion for Robustness Against Growth Feedback

The quantitative measure $R(k_g)$ we have introduced to characterize the effects of growth feedback on gene circuit functioning is generally not amenable to analytic treatment. However, for weak feedback, certain analytic insights can still be gained. Here we consider a three-node gene circuit designed to have adaptation and analyze how growth feedback destroys adaptation. We focus on type-I failure, where the growth feedback makes $O_2(C)$ deviate from $O_1(C)$, because (1) this type of failures is arguably the most important type as it alone takes nearly half of all the failures, and (2) it can be analyzed. Here we provide a semi-quantitative analysis to elucidate how a small $k_g > 0$ can make $O_2(C)$ deviate from $O_1(C)$.

Circuit robustness in the absence of growth feedbac

The dynamical equations of the circuit in the absence of growth feedback are:

$$\frac{dA}{dt} = f_A = G_A - d_A A, \tag{15}$$

$$\frac{dB}{dt} = f_B = G_B - d_B B, \tag{16}$$

$$\frac{dC}{dt} = f_C = G_C - d_C C, \tag{17}$$

Where

$$G_A = H_{\text{Input},A}(\text{Input}) \cdot H_{A,A}(A) \cdot H_{B,A}(B) \cdot H_{C,A}(C), \tag{18}$$

and each H term represents the regulation of a single link in the circuit. The steady-state solutions (A_0, B_0, C_0) are given by

$$A_0 = G_A/d_A \tag{19}$$

$$B_0 = G_B/d_B \tag{20}$$

$$C_0 = G_C/d_C. \tag{21}$$

For notation convenience, we use x to denote an arbitrary node (A, B, or C). The steady-state solutions can thus be written as

$$x_0 = G_x/d_x. \tag{22}$$

With a small input signal change ΔI applied to the circuit, the steady states becomes ($A_0 + \Delta A_0$, $B_0 + \Delta B_0$, $C_0 + \Delta C_0$). Under ΔI, the dynamical equations at the steady point can be written as

$$0 = f_x(y_0 + \Delta y_0, \text{input} = \Delta I). \tag{23}$$

For $\Delta I = 0$, the equation becomes

$$0 = f_x(y_0, \text{input} = 0). \tag{24}$$

Subtracting *Eq. (24)* from *Eq. (23)*, we get

$$\begin{bmatrix} 0 \\ 0 \\ 0 \end{bmatrix} = \mathcal{J}_f \begin{bmatrix} \Delta A_0 \\ \Delta B_0 \\ \Delta C_0 \end{bmatrix} + \begin{bmatrix} \frac{\partial f_A}{\partial I} \\ 0 \\ 0 \end{bmatrix} \Delta I, \tag{25}$$

Where

$$\mathcal{J}_f = \begin{bmatrix} \frac{\partial f_A}{\partial A} & \frac{\partial f_A}{\partial B} & \frac{\partial f_A}{\partial C} \\ \frac{\partial f_B}{\partial A} & \frac{\partial f_B}{\partial B} & \frac{\partial f_B}{\partial C} \\ \frac{\partial f_C}{\partial A} & \frac{\partial f_C}{\partial B} & \frac{\partial f_C}{\partial C} \end{bmatrix} \tag{26}$$

is the Jacobian matrix of the original dynamical equations evaluated at (A_0, B_0, C_0).

Solving *Eq. (25)*, we have

$$\begin{bmatrix} \Delta A_0 \\ \Delta B_0 \\ \Delta C_0 \end{bmatrix} = -\mathcal{J}_f^{-1} \begin{bmatrix} \frac{\partial f_A}{\partial I} \\ 0 \\ 0 \end{bmatrix} \Delta I \tag{27}$$

For the steady state to remain stable under ΔI, the requirement is that ratio $\Delta C_0/\Delta I$ be small. Assuming that the Jacobian matrix satisfies the conditions to make points (A_0, B_0, C_0) and ($A_0 + \Delta A_0$, $B_0 + \Delta B_0$, $C_0 + \Delta C_0$) stable in their corresponding dynamical systems, we have

$$\frac{\Delta C_0}{\Delta I} = \left(-\mathcal{J}_f^{-1} \begin{bmatrix} \frac{\partial f_A}{\partial I} \\ 0 \\ 0 \end{bmatrix} \right)_3, \tag{28}$$

where $(\cdot)_3$ denotes the third component of the vector inside. The limiting case of a perfectly precise circuit is defined to be $\Delta C_0/\Delta I = 0$, yielding a precision criterion of by $((\mathcal{J}_f^{-1})_{31} \approx 0)_{31} \approx 0$ or

$$\left(\frac{\partial f_B}{\partial A} \frac{\partial f_C}{\partial B} - \frac{\partial f_B}{\partial B} \frac{\partial f_C}{\partial A} \right) / \text{Det}(\mathcal{J}_f) \approx 0. \tag{29}$$

leading to

$$\frac{\partial f_B}{\partial A} \frac{\partial f_C}{\partial B} - \frac{\partial f_B}{\partial B} \frac{\partial f_C}{\partial A} = 0. \tag{30}$$

which is the central criterion analyzed in **Shi et al.** (**2017**). The two families, NFBL and IFFL, satisfy this same criterion through different mechanisms.

Precision criteria in the presence of weak growth feedback and $J \to \infty$

We now incorporate growth feedback into the analysis in the limit $J \to \infty$. In this case, the burden b is small so that the dilution strength can be approximated as $dN/dt/N \approx k_g$. Suppose weak growth feedback is present before and after the small input signal ΔI is applied. Let the steady state under growth feedback before application of ΔI be denoted as (A_0', B_0', C_0'). The steady state with input ΔI can be written as $(A_0' + \Delta A_0', B_0' + \Delta B_0', C_0' + \Delta C_0')$.

The basic equations before and after application of ΔI are

$$\frac{dx'}{dt} = f_x(y', \text{input} = 0) - k_g x', \tag{31}$$

$$\frac{d(x' + \Delta x')}{dt} = f_x(y' + \Delta y', \text{input} = \Delta I) - k_g(x' + \Delta x'). \tag{32}$$

Subtracting *Eq. (31)* from *Eq. (32)*, we get

$$\begin{bmatrix} 0 \\ 0 \\ 0 \end{bmatrix} = (\mathcal{J}_f' - k_g \mathcal{I}) \begin{bmatrix} \Delta A' \\ \Delta B' \\ \Delta C' \end{bmatrix} + \begin{bmatrix} \frac{\partial f_A}{\partial I} \\ 0 \\ 0 \end{bmatrix} \Delta I, \tag{33}$$

where $\mathfrak{I}$ is the identity matrix. The solution is

$$\begin{bmatrix} \Delta A' \\ \Delta B' \\ \Delta C' \end{bmatrix} = -(\mathcal{J}_f' - k_g \mathcal{I})^{-1} \begin{bmatrix} \frac{\partial f_A}{\partial I} \\ 0 \\ 0 \end{bmatrix} \Delta I. \tag{34}$$

Compared with *Eq. (27)*, the differences are that the matrix $\mathcal{J}_\leq$ is replaced by $(\mathcal{J}_f' - k_g \mathcal{I})$, and x, Δx are replaced by x', $\Delta x'$, respectively.

The precision criterion again requires $\Delta C_0'/\Delta I$ to be small. we have

$$\frac{\Delta C_0'}{\Delta I} = \left(-(\mathcal{J}_f' - k_g \mathcal{I})^{-1} \begin{bmatrix} \frac{\partial f_A}{\partial I} \\ 0 \\ 0 \end{bmatrix} \right)_3, \tag{35}$$

which is equivalent to

$$((\mathcal{J}_f' - gE)^{-1})_{31} = \left[\frac{\partial f_B}{\partial A} \frac{\partial f_C}{\partial B} - (\frac{\partial f_B}{\partial B} - k_g) \frac{\partial f_C}{\partial A} \right]_{A', B', C'} / \text{Det}(\mathcal{J}_f' - gI) \approx 0, \tag{36}$$

leading to

$$\left[\frac{\partial f_B}{\partial A} \frac{\partial f_C}{\partial B} - (\frac{\partial f_B}{\partial B} - k_g) \frac{\partial f_C}{\partial A} \right]_{A', B', C'} \approx 0. \tag{37}$$

Comparing this equation for precision criterion *Eq. (37)* ⊡ with the criterion *Eq. (30)* ⊡ in the absence of growth feedback, we find an extra term of k_g. This explicit term of k_g makes the criterion more difficult to satisfy with a range of different k_g values. It requires either $\partial f_C / \partial A$ is zero or the four partial derivative terms change accordingly with a varying k_g to have exact cancellations.

For neither the NFBL nor the IFFL family, $\partial f_C / \partial A = 0$ can be satisfied. In none of the 425 network topologies, the link from node A to node C is absent ($\partial f_C / \partial A = 0$). Thus with a random sampling of the parameters for the circuits that have adaptation at $k_g = 0$, the probability that $\partial f_C / \partial A = 0$ can occur is negligibly small.

Precision criterion with exact cancellations for the optimal family

As the criterion $\partial f_C / \partial A = 0$ cannot be satisfied in three-node gene circuits, we discuss the possibility of exact cancellations with varying k_g. For the optimal circuit family demonstrated in **Fig. 5(b)** ⊡, we have $\partial f_C / \partial B = 0$ as there is no direct link from node B to node C. The precision criterion becomes

$$\left[\left(\frac{\partial f_B}{\partial B} - k_g \right) \frac{\partial f_C}{\partial A} \right]_{A_0', B_0', C_0'} \approx 0. \tag{38}$$

Since $\partial f_C / \partial A \neq 0$, this can be rewritten as

$$\frac{\partial f_B}{\partial B} \Big|_{A_0', B_0', C_0'} - k_g \approx 0. \tag{39}$$

For this family, the precision criterion in the absence of growth feedback is

$$\frac{\partial f_B}{\partial B} \Big|_{A_0, B_0, C_0} \approx 0. \tag{40}$$

Combining **Eqs. (39** ⊡ **-40** ⊡ **)**, we get

$$\frac{\partial^2 f_B}{\partial A \partial B} \Big|_{A_0, B_0, C_0} (A_0' - A_0) + \frac{\partial^2 f_B}{\partial C \partial B} \Big|_{A_0, B_0, C_0} (C_0' - C_0)$$
$$\approx k_g. \tag{41}$$

Using the approximation employed in **Shi et al**. (**2017**) for the NFB family that f_B is a linear function of B, we have

$$\frac{\partial f_B(A, B, C)}{\partial B} \approx \frac{f_B(A, B, C)}{B}$$
$$= \frac{v_B}{K_{BB}} H_{A,B}(A) H_{C,B}(C) - d_B. \tag{42}$$

We thus have

$$\frac{d H_{A,B}(A)}{d A} \Big|_{A_0} H_{C,B}(C_0)(A_0' - A_0) + H_{A,B}(A_0) \frac{d H_{C,B}(C)}{d C} \Big|_{C_0} (C_0' - C_0) \approx \frac{K_{BB}}{v_B} k_g. \tag{43}$$

This equation can be solved analytically only in the regime of $k_g \sim 0$ where ($(A_0' - A_0)$) and ($(C_0' - C_0)$) are approximately linear functions of k_g. But it should be difficult for the circuit to meet this criterion with a random sampling of the circuits that have adaptation at $k_g = 0$.

Appendix 2

Network motifs supporting oscillations

As summarized in *Novák and Tyson* (*2008*), three classes of motifs can support oscillations in a three-node circuit.

Class 1 (the dominant class)

Delayed negative-feedback loop with an intermediate node in the path of the negative feedback loop. A majority of the networks with an oscillation-supporting motif belong to this class (237 out of 245 networks). All the circuits that have more than 20% failures as oscillation-induced failures belong to this class.

Class 2

Amplified negative-feedback loop, with a node regulated by both a negative-feedback loop through another node and a positive-feedback loop through the third node. There are only 8 network topologies that fall into this class. They result in 3% to 20% oscillation-induced failures.

Class 3

Incoherently amplified negative-feedback loops, as demonstrated in **Fig. 5(c)** ⧉ of *Novák and Tyson* (*2008*). Among all the 425 networks capable of adaptation studied in our work, no network belongs to this class.

Appendix 3

Self-activation and toggle switch circuits

The key quantitative results about the survival ratio $R(k_g)$ presented in the main text are obtained from various circuit topologies with three genes. To demonstrate the general applicability of $R(k_g)$, we study two simpler gene circuits: a self-activation circuit with a single gene and a toggle switch circuit with two genes. A comparative study of these two classes of circuits has been carried out recently (*Zhang et al., 2020* ⧉), whose topological structures are shown in **Figs. 1(a1)** ⧉ and **1(a2)** ⧉, respectively. In the absence of growth feedback, both networks exhibit bistability and a hysteresis loop. Under dilution, the self-activation circuit quickly loses the memory while the toggle switch circuit can remain functional, as was observed numerically and experimentally (*Zhang et al., 2020* ⧉).

Our simulation settings are mostly identical to that of 3-node circuits in the main text, including the sampling regions of the random circuit parameters, the specifics of the ODE solver, and the criterion for locating equilibrium. We set $J = 1$. Other than the network topology, the only difference is the functionality criteria. Here, the desired function is a hysteresis. We test the response of the circuit output when (i) the input is a switch from an off-state (with input signal $I_{off} = 10^{-8}$) to an on-state (with input signal $I_{on} = 2$) and (ii) the input is switched from an on-state to an off-state. In the former trial, the steady-state output is switched from $O_{1,off}$ to $O_{1,on}$, while in the latter it is switched from $O_{2,on}$ to $O_{2,off}$. The criteria are: (i) the two steady states are distinguishable: $\Delta O = O_{2,on} - O_{1,off} > 0.1$; and (ii) the system exhibits a hysteresis: $(O_{1,on} - O_{1,off})/\Delta O > 0.5 > (O_{2,on} - O_{2,off})/\Delta O$.

Figures 1(b1) ⧉ and **1(b2)** ⧉ show the scaling law of $R(k_g)$ with k_g for the self-activation and toggle switch circuits, respectively. It can be seen that, for the self-activation circuit, as the growth feedback strength increases, $R(k_g)$ approaches zero quickly, indicating that the circuit function
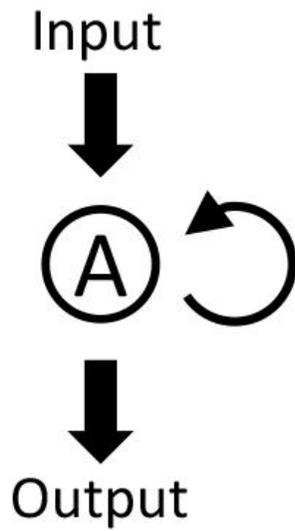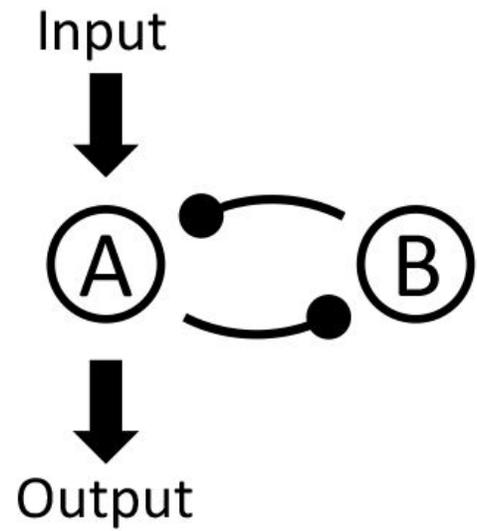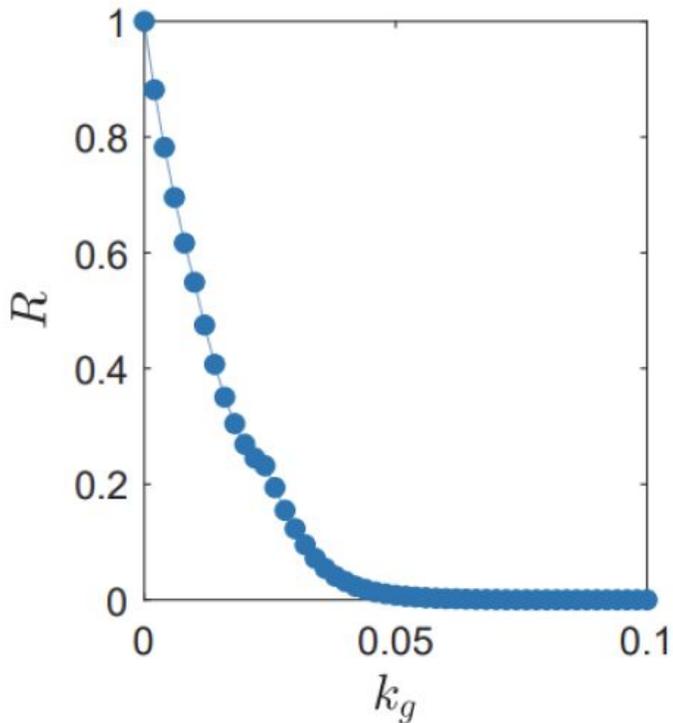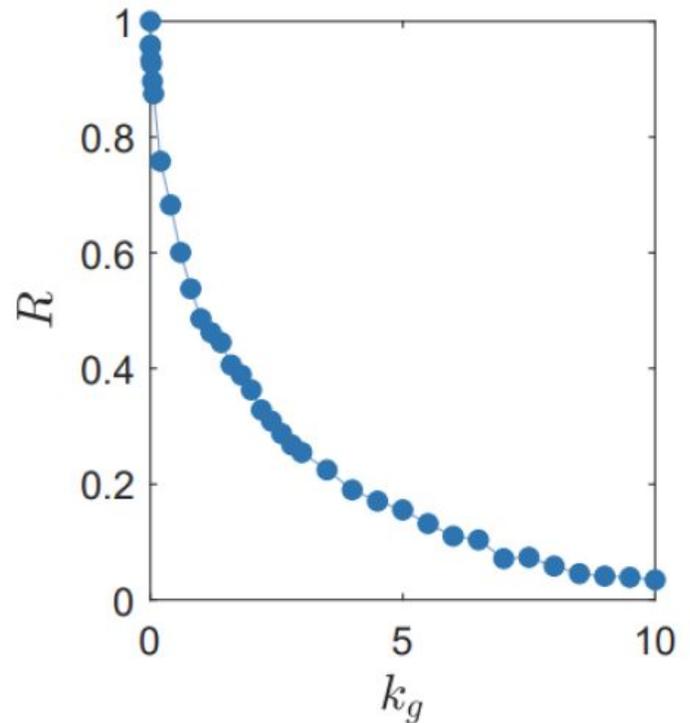
Appendix 3–figure 1.

Scaling law of robustness measure for the single-gene self-activation circuit and the two-gene toggle switch circuit. (a1,b1) The topology of the self-activation circuit and the decay of the robustness measure with the growth feedback strength. (a2,b2) Same legends as (a1,b1), respectively, for the toggle switch circuit. Note the drastic difference in the range of k_g values in (b1) and (b2) where R approaches zero much more quickly in the former than in the latter, indicating the nearly immediate loss of functions of the single-gene circuit even under weak growth feedback.

cannot sustain even weak feedback with near zero strength. For the toggle switch, $R(k_g)$ approaches zero eventually but at a much slower rate, a result that is consistent with the finding in ***Zhang et al.*** (***2020***). Remarkably, the scaling of $R(k_g)$ with k_g exhibits qualitatively similar behavior as the scaling laws reported in the main text for various three-gene circuits, lending further credence for the general applicability of the quantitative measure $R(k_g)$ to characterize the effects of growth feedback on gene networks.

Appendix 4

Regularized feed-forward neural networks for identifying critical links

We employed ensembles of regularized feed-forward neural networks to detect, in an automated fashion, the links that are crucial in determining the level of robustness R. The neural-network structure is illustrated in **Fig. 6(e)** ⧉, which has three layers: an input layer, a hidden layer, and an output layer. The input layer receives a nine-dimensional circuit topology vector where each entry represents a potential link in the three-node circuit, such as $A \rightarrow A$ and $B \rightarrow C$. For an activation (inhibition) link, the entry value is set to +1 (−1). In the absence of such a link, the value is zero. In the hidden layer, there are only two neurons that use a hyperbolic tangent activation function, creating a bottleneck that limits the complexity of the extracted features. The output layer has one neuron that uses a hyperbolic tangent activation function trained to output the estimated robustness $\hat{R}$. The input and hidden layers are connected by the matrix W_{in}, and the hidden and output layers are connected by the matrix W_{out}. Given the input vector u, the estimated $\hat{R}$ can be expressed as

$$\hat{R} = \tanh[W_{\text{out}} \tanh(W_{\text{in}} u)]. \tag{44}$$

We use all the 303 circuit topologies that have $Q(k_g = 0) > 100$ for training to minimize the relative random fluctuations in the training data. The loss function for optimization is

$$\text{Loss} = |\hat{R} - R| + \beta \sum_{i=1}^{w_h} \sum_{j=1}^{L_n} |W_{\text{in},ij}|, \tag{45}$$

where $\beta = 0.05$ is the l-1 regularization coefficient, $L_n = 9$ is the number of possible links within a three-gene circuit, and $w_h = 2$ is the width of the hidden layer. We train the network using a stochastic gradient descent algorithm and repeat it 50 times with different initial weights in the neural net matrices. The "importance" of a link is determined by the logarithm of the absolute value of the weights in W_{in} corresponding to the gain of that link. This importance measure is then averaged over all 50 neural networks.

Appendix 5

Lack of correlation between the circuit robustness and topological families

As shown in **Fig. 1** ⧉, the network topologies belonging to the two different families (marked in different colors) are mingled together and spread all over the range of $R(k_g)$, suggesting no significant correlation between the circuit robustness and circuits family. To quantify this irrelevance, we calculate the point biserial correlation between (a) the $R(k_g)$ values of all the network topologies with $Q(k_g = 0) \leq 200$ (to lower the fluctuations) and (b) a binary variable b_f
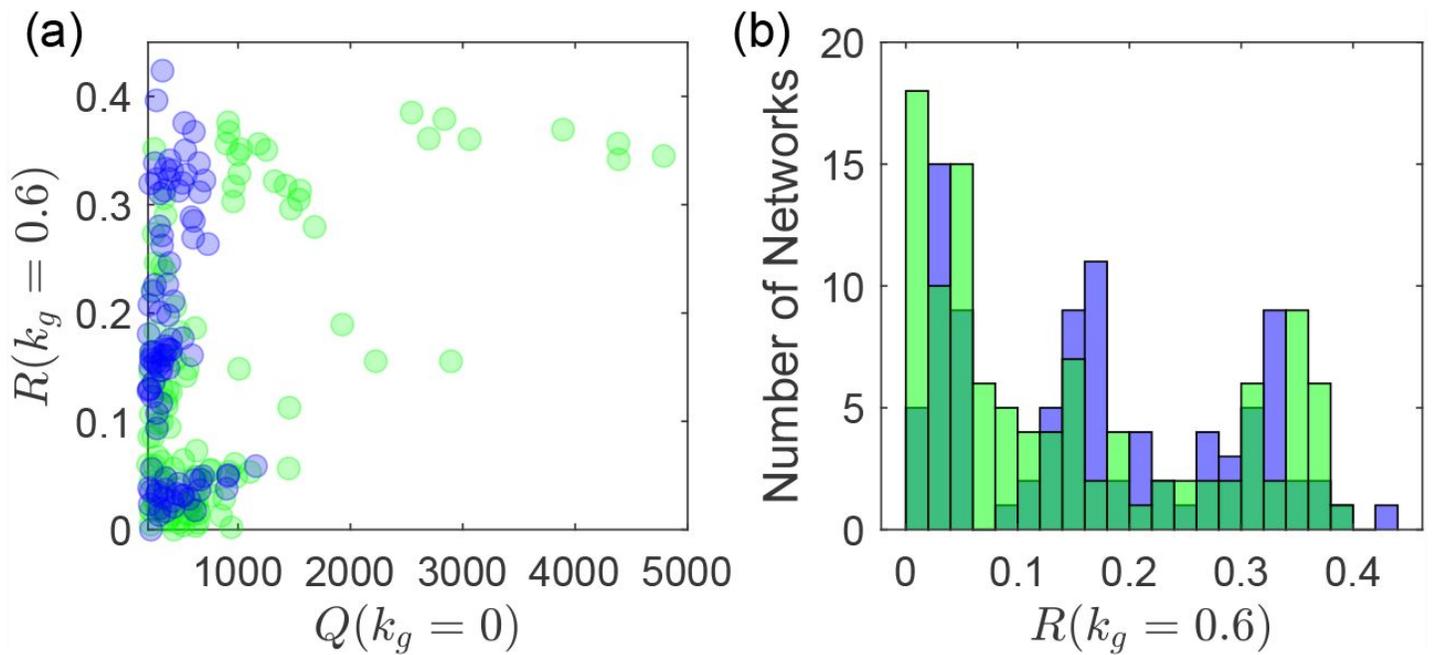
Appendix 5–figure 1.

Demonstration of circuit robustness against growth feedback being unrelated to NFBL or IFFL family membership. The green and blue colors represent the NFBL and IFFL families, respectively. (a) Robustness measure $R(k_g = 0.6)$ versus $Q(k_g = 0)$, where each node represents a network topology. Circuits from both families are widely distributed across different levels of R and intermingled. (b) Distributions of $R(k_g = 0.6)$ for the two families, which are quite similar.

which is $b_f = 0$ for the NFBL family and $b_f = 0$ for the IFFL family. The calculation involves 108 NFBL network topologies and 93 IFFL topologies. The resulting point biserial correlation is as small as 0.1. The 95% confidence interval for the true difference with respect to the two families of $R(k_g)$ is $(-0.01, 0.06)$, which is narrow around zero.

Appendix 6

Results from low burden level

For the simulation results reported in the main text, the burden parameter is fixed at $J = 1$. What are the possible behaviors of the gene circuit for different values of J? Suppose J is much larger than one. In this case, the burden term b that has J in the denominator is negligible, thereby reducing the complexity of the system and providing a parameter regime in which the contributing factors to the survival ratio $R(k_g)$ other than the burden can be identified.

In the regime of large J, the burden in **Eq. (8)** ⤢ in the main text is much smaller than one, so **Eq. (7)** ⤢ in the main text about growth rate can be simplified as

$$\frac{dN}{dt} = k_g \frac{1}{1+b} N = k_g \frac{1}{1 + (A + B + C)/J} N \approx k_g N, \qquad (46)$$

indicating that cell growth is determined entirely by the growth-feedback strength k_g. It can be seen from **Eqs. (4** ⤢-**6** ⤢) in the main text that, in this case, the effect of growth feedback is equivalent to a linear change of the amount k_g in the degradation terms d_x. Further, the interaction between cell growth and the gene circuit is no longer of the type of mutual inhibition: the regulation is a one-way interaction from cell growth to the gene circuit. A semi-quantitative analysis of this scenario can be found in **Appendix 1** ⤢.

We carry out the simulations as in the main text in the regime of large J and perform a comparative analysis of the results.

The first issue concerns the relative fractions of different failure scenarios. **Figure 1** ⤢ compares the distributions of distinct types of circuit failures for $J = 1$ and $J \to \infty$. The possible failure scenarios are identical in both cases, in spite of the quantitative differences in the relative fractions of the failure mechanisms. Some of the differences are sizable, but none is significant in the sense that none is beyond an order of magnitude. For example, for $J = 1$, type-I failures are the most common (49%) where the precision criterion is broken in a continuous fashion. For $J \to \infty$, the fraction is about 31%, but the reduction is still within a factor of two. The plausible reason for the reduction is that the additional regulation of the burden b for $J = 1$ is more difficult to be maintained (**Appendix 1** ⤢).

The second issue is the scaling law between the survival ratio $R(k_g)$ and the growth-feedback strength k_g. **Figure 2** ⤢ compares the scaling laws of $R(k_g)$ for three circuit topologies for $J = 1$ and $J \to \infty$, where the results in **Figs. 2(a1)** ⤢ and **2(a2)** ⤢ are represented on a linear scale, while those in **Figs. 2(b1)** ⤢ and **2(b2)** ⤢ are on a double-logarithmic versus logarithmic scale. The approximately linear relation in **Fig. 2(b2)** ⤢ suggests that, for $J \to \infty$, the scaling laws is given by (1) in the main text.

For $J = 1$, the scaling law (1) is less accurate, as shown in **Fig. 2(b1)** ⤢, which can be heuristically explained, as follows. Suppose we use **Eq. (46)** ⤢ and reduce J from a large value to one, which is equivalent to adding back the negative feedback from the burden $b = A + B + C$ to cell growth. Since cell growth effectively inhibits the gene regulation in the circuit, the burden will be larger for smaller values of k_g, suppressing the cell growth. Thus, for weak growth feedback
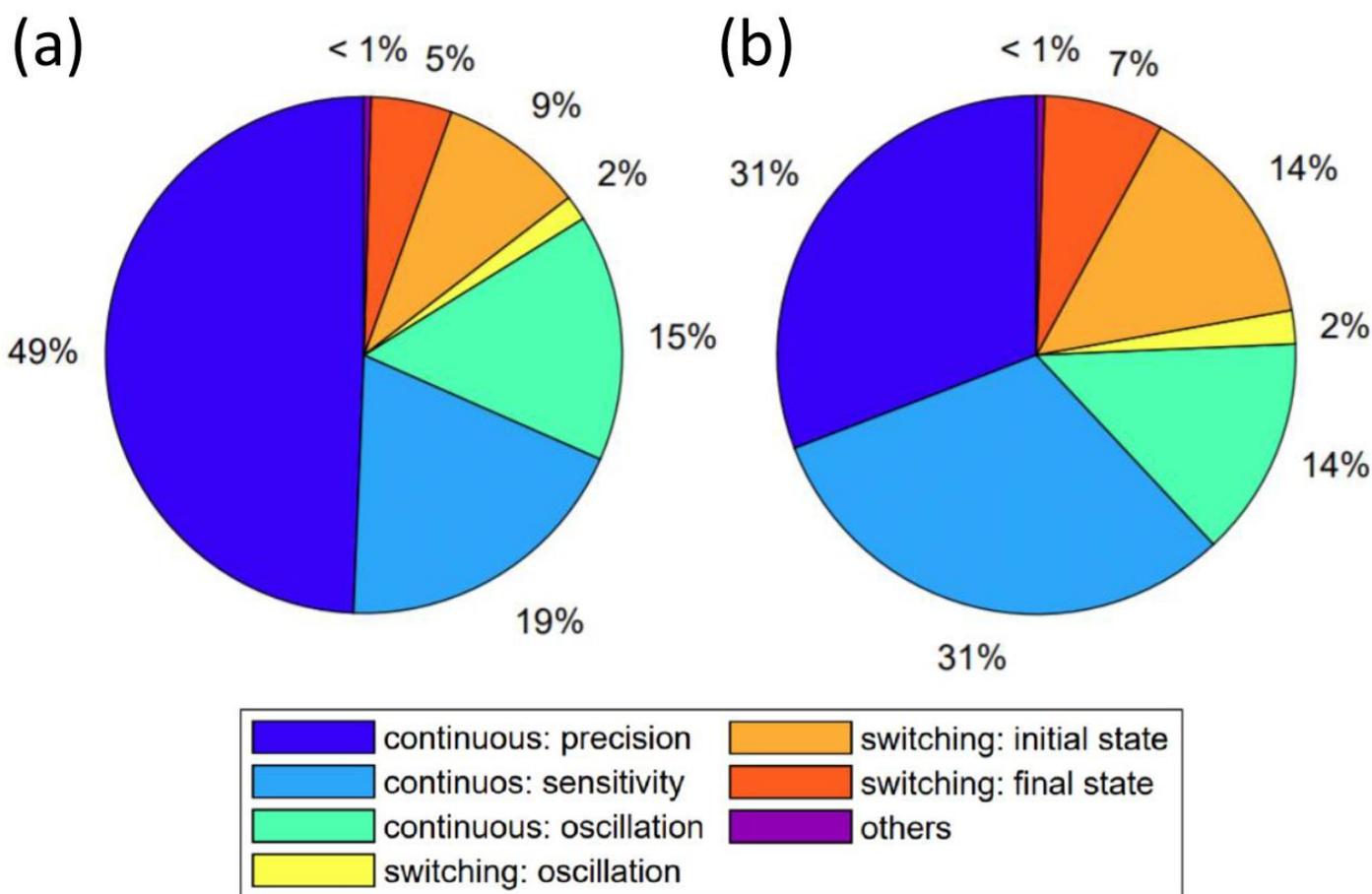
Appendix 6–figure 1.

Circuit performance for zero burden. Shown is a comparison of the distributions of circuit failure scenarios under growth feedback for (a) $J = 1$ as in the main text and (b) $J \to \infty$ (zero burden). In both cases, there are six categories in spite of some quantitative differences in their probabilities, implying that, as the burden is reduced to zero from a finite value continuously, the failure scenarios are qualitatively the same. Notable is the fraction of circuits suffering type-I failures (violation of the precision criterion), which has a relatively large reduction for $J \to \infty$, a result that is consistent with the semi-quantitative analysis in Appendix 1.
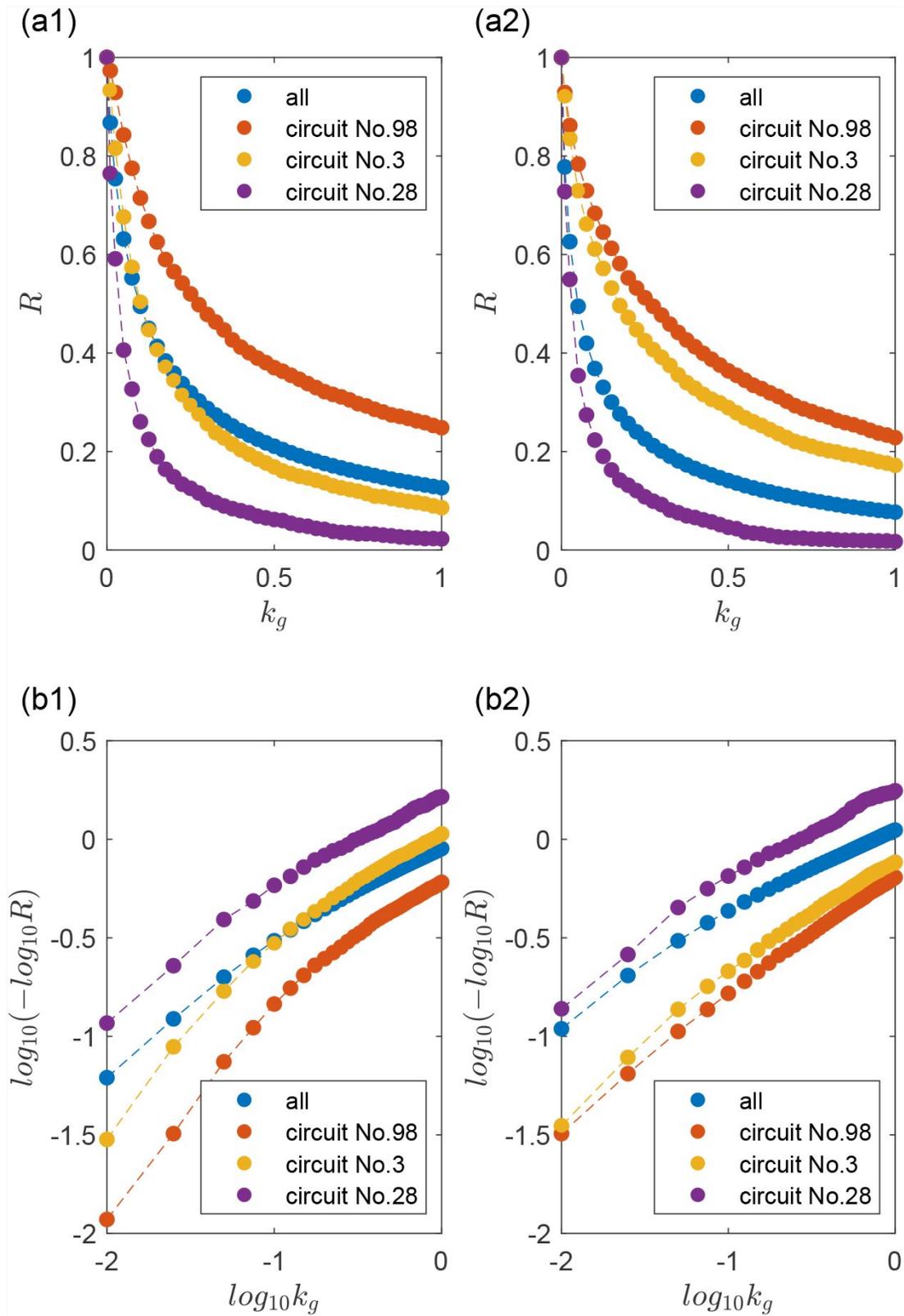
Appendix 6–figure 2.

Scaling law of circuit robustness measure for zero burdens. (a1,b1) Representative scaling relations between $R(k_g)$ and k_g for $J = 1$ as in the main text, plotted on two different scales. (a2,b2) Representative scaling relations for $J \to \infty$. The curves in (b2) are approximately linear, suggesting the scaling law (1) in the main text. In (b1), the curves are less linear where the added burden leads to more reduction in $R(k_g)$ in the regime of weak growth feedback.

(corresponding to small values of k_g), for small J, $R(k_g)$ decreases more slowly than for larger values of J. The difference becomes smaller for larger values of k_g, causing the curves on the left side in **Fig. 2(b1)** ⬀ to be lower than those in **Fig. 2(b2)** ⬀, but the curves on the right side are similar in both cases.

The third issue is the effect of the network topology on the survival ratio $R(k_g)$. **Figure 3** ⬀ presents a comparison of the dependency of R on the circuit topology for $J = 1$ and $J \to \infty$. As discussed above, the difference in the burden b can be a major reason for the data points in the red group to have lower R values compared with those in the blue and green groups. When the term b is effectively removed by setting $J \to \infty$, the difference diminishes. It can be seen from **Figs. 3(a2)** ⬀, **3(b2)** ⬀ and **3(c2)** ⬀ that, in this case, the range of R for the red group, in spite of the low R values, overlaps with that of the blue group. However, the R values associated with the red group are still distinctly smaller than those with the green group, suggesting some characteristic differences in the network motifs that define these two groups.

Figures 3(b1) ⬀ and **3(b2)** ⬀ indicate a persistent feature of the distribution of the survival ratio $R(k_g = 0.6)$ for the ensemble of networks: there are three peaks regardless of whether J has a small or a large value. Further, the three peaks are approximately located at the same positions for $J = 1$ and $J \to \infty$. This feature provides a criterion to determine the likelihood of a given network topology being stable or unstable under growth feedback without the need to calculate the $R(k_g)$ value for many values of the feedback strength. In particular, if the network is such that its $R(k_g = 0.6)$ value is associated with the red peak, then it is highly likely to be unstable and fail to function under growth feedback. On the contrary, if a network "belongs" to the green peak, then the chance for it to sustain its function in a growth environment will be improved significantly.

There can be two different mechanisms for growth-induced oscillations: (i) by altering the system parameter, and (ii) by altering the circuit topology with the additional dynamical variable N and regulations attached to it. Our results suggest the first mechanism is the major one, while the second one does not appear to play a significant role. The second mechanism only exists with a finite J. Thus, we compare the cases of $J = 1$ and the limit of a large J. As shown in **Fig. 3** ⬀, the ratio of functional failures caused by growth-induced oscillations does not change much between the two cases. However, the oscillatory behavior is sensitive to the value of the dilution parameter. In order to have oscillations, it is necessary that the parameter be in some specific interval (***Novák and Tyson, 2008*** ⬀).

Appendix 7

Four-gene circuits

To demonstrate the general applicability of our nonlinear dynamical analysis of the failure mechanism, we study four-gene circuits. **Figure 1(a)** ⬀ shows ten representative circuits, where eight are from ***Qiao et al.*** (***2019***) and two being the four-node modifications of three-gene circuits with oscillation-related motifs. For each circuit, we test 10^5 random sets of parameters. To generate acceptable statistics, we ease the precision and sensitivity criteria to: (i) $|(O_2 - O_1)/O_1| < 0.4$, (ii) $O_{\text{peak}} > 0.1$, and (iii) $O_{\text{peak}}/O_1 > 0.5$ or $O_{\text{peak}}/O_1 - |(O_2 - O_1)/O_1| > 0.1$. All other simulation settings are the same as those in the three-gene circuit simulations as detailed in the main text. We collect a total of 3,275 trials exhibiting functional adaptation in the absence of growth feedback ($k_g = 0$). As the growth feedback is turned on so that $k_g = 0$ increases $k_g = 0.5$, 2,373 trials encountered functional failures across all ten circuits.

We then investigate the causes of the functional failures. We find that all 2,373 trials fall into the same three categories identified for three-gene circuits: growth-induced oscillations, growth-induced switching in bistability, and continuous deformation of the system trajectory leading the
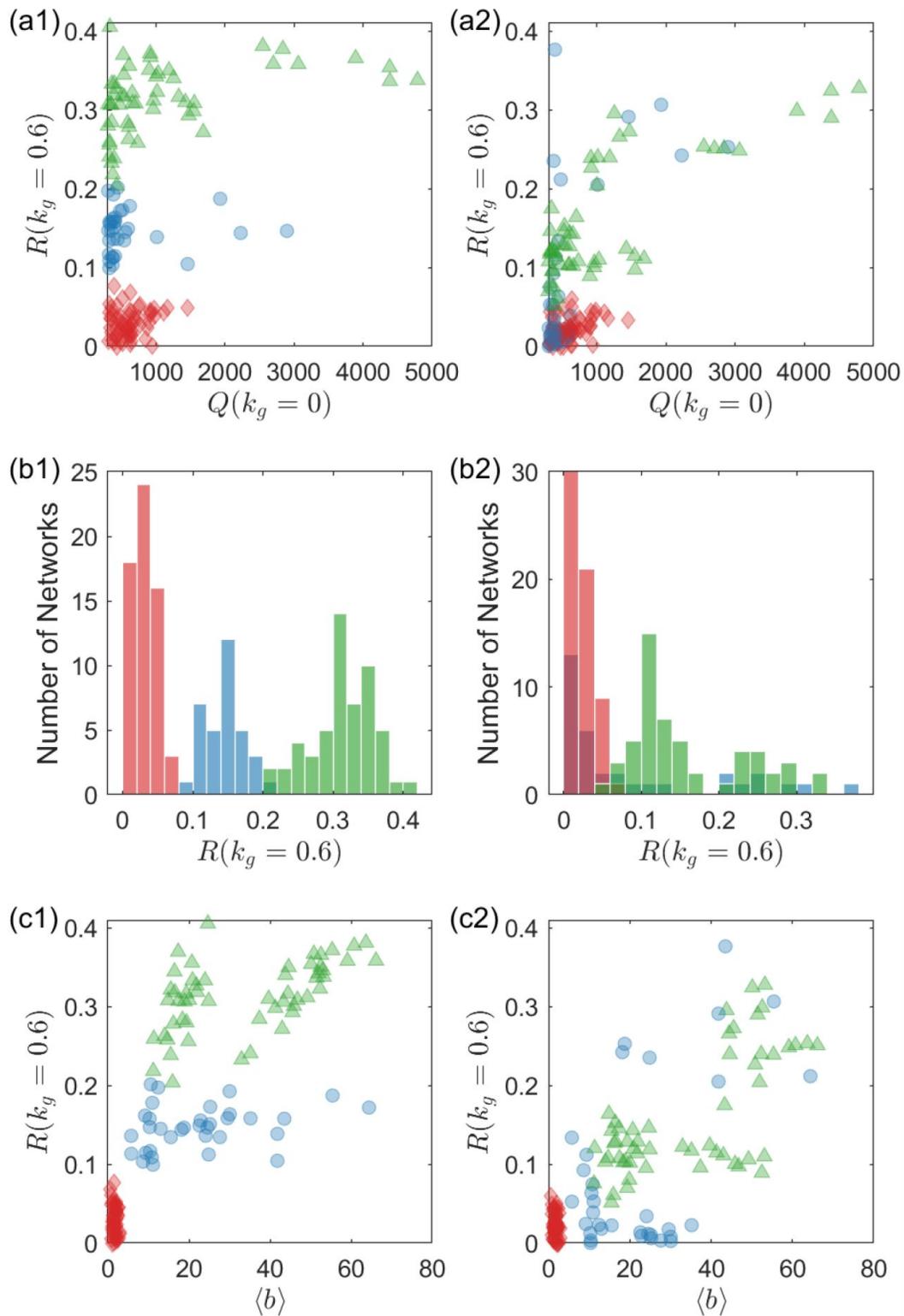
Appendix 6–figure 3.

Dependence of the distribution of the robustness measure $R(k_g = 0.6)$ on circuit topology. (a1) For $J = 1$ (as in the main text), $R(k_g = 0.6)$ versus $Q(k_g = 0)$ (a quantity that measures the likelihood of a functional circuit) for all 425 network topologies. (b1) Histogram of $R(k_g = 0.6)$ for $J = 1$ constructed from all network topologies. (c1) $R(k_g = 0.6)$ versus the burden parameter. In (a1-c1), each data point represents a specific network topology. (a2-c2) The same legends as in (a1-c1), respectively, for $J \rightarrow \infty$. For diminishing burden, the circuit topologies associated with the red group remain to be more unstable comparing with those in the green group.
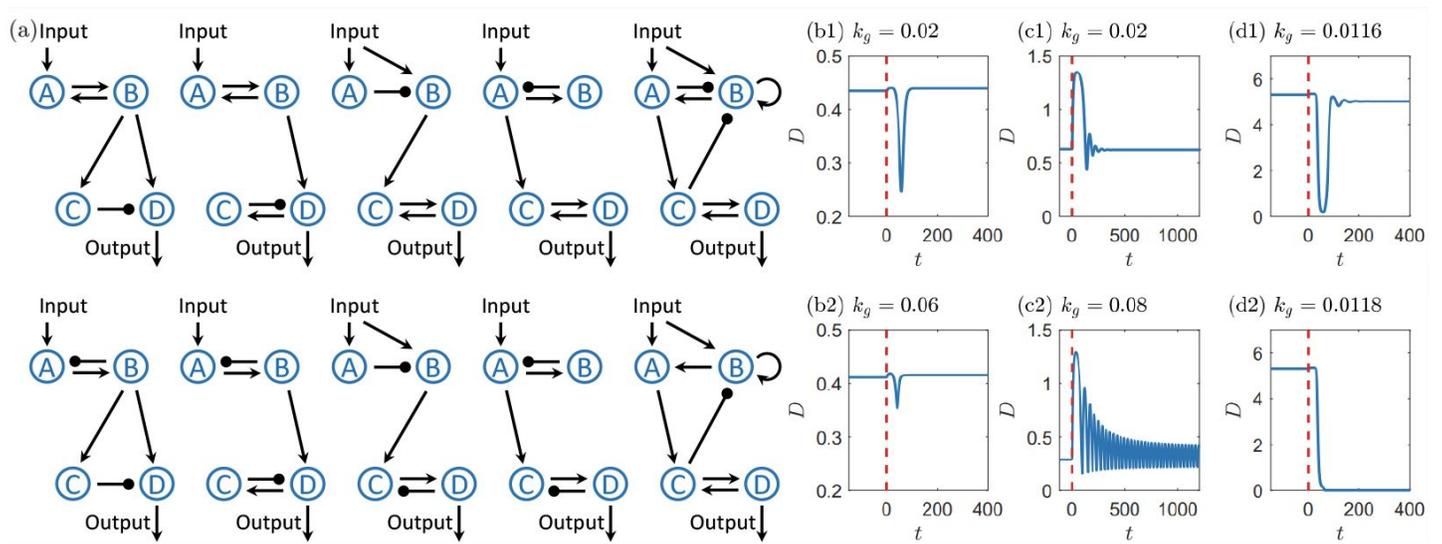
Appendix 7–figure 1.

(a) Ten representative four-gene circuits. The eight circuits in the first four columns are from ***Qiao et al.*** (***2019***), and the two circuits in the fifth column are selected due to the oscillation-related motifs in their topologies and the relatively high $Q(k_g = 0)$ values when reduced to three-gene circuits. (b-d) Examples of the three major categories of growth-feedback induced functional failures in the four-gene circuits, where the upper panels display the circuit outputs with smaller k_g values for which the circuits remain functional and the lower panels showcase the circuit outputs with larger k_g values for which the circuits lose their functionality. The vertical red dashed line marks the time when the input is switched to another state. The three failure categories are identical to these in the three-gene circuits in the main text: (b1, b2) continuous trajectory deformation causing the system to cross thresholds associated with the sensitivity criterion, (c1, c2) growth-strengthened oscillations, and (d1, d2) growth-induced switching in bistability. The change in k_g between panels (d1) and (d2) is small so as to show the abrupt change in the response at a critical point.

system to cross the criteria thresholds, as shown in **Figs. 1(b-d)** ⬀ , respectively. For the cases studied, continuous deformation is the dominant failure mechanism, accounting for about 88% of the failures. The fractions of oscillation-related and bistability-related failures are approximately 10% and 3%, respectively. These results indicate that four-gene and three-gene circuits share the common mechanisms of growth-feedback induced failures, implying the generality of these failure mechanisms.

References

Aoki SK, Lillacci G, Gupta A, Baumschlager A, Schweingruber D, Khammash M. (2019) **A universal biomolecular integral feedback controller for robust perfect adaptation** *Nature* **570**:533–537

Bello I, Pham H, Le QV, Norouzi M, Bengio S. (2016) **Neural combinatorial optimization with reinforcement learning** *arXiv*

Boo A, Ellis T, Stan GB (2019) **Host-aware synthetic biology** *Cur Opin Sys Biol* **14**:66–72

Borkowski O, Ceroni F, Stan GB, Ellis T. (2016) **Overloaded and stressed: whole-cell considerations for bacterial syn-thetic biology** *Current Opinion in Microbiology* **33**:123–130 https://doi.org/10.1016/j.mib.2016.07.009

Briat C, Gupta A, Khammash M. (2016) **Antithetic integral feedback ensures robust perfect adaptation in noisy biomolecular networks** *Cell Sys* **2**:15–26

Caliando BJ, Voigt CA (2015) **Targeted DNA degradation using a CRISPR device stably carried in the host genome** *Nature communications* **6**:1–10

Ceroni F, Algar R, Stan GB, Stan GB, Stan GB, Ellis T, Ellis T, Ellis T. (2015) **Quantifying cellular capacity identifies gene expression designs with reduced burden** *Nature Methods* **12** https://doi.org/10.1038/nmeth.3339

Ceroni F, Boo A, Furini S, Gorochowski TE, Borkowski O, Ladak YN, Awan AR, Gilbert C, Stan GB, Ellis T. (2018) **Burden-driven feedback control of gene expression** *Nature Methods* **15**:387–393 https://doi.org/10.1038/nmeth.4635

Darlington APS, Kim J, Jimenez JI, Bates DG (2018) **Engineering Translational Resource Allocation Controllers: Mech-anistic Models, Design Guidelines, and Potential Biological Implementations** *ACS Synth Biol* **7**:2485–2496 https://doi.org/10.1021/acssynbio.8b00029

Darlington APS, Kim J, Jiménez JI, Bates DG (2018) **Dynamic allocation of orthogonal ribosomes facilitates uncoupling of co-expressed genes** *Nature Communications* **9** https://doi.org/10.1038/s41467-018-02898-6

Deris JB, Kim M, Zhang Z, Okano H, Hermsen R, Groisman A, Hwa T. (2013) **The innate growth bistability and fitness landscapes of antibiotic-resistant bacteria** *Science* **342**

Elowitz MB, Leibler S. (2000) **A synthetic oscillatory network of transcriptional regulators** *Nature* **403**:335–338

Feng J, Kessler DA, Ben-Jacob E, Levine H. (2014) **Growth feedback as a basis for persister bistability** *Proc Nat Aca Sci* **111**:544–549

Ferrell Jr JE (2016) **Perfect and near-perfect adaptation in cell signaling** *Cell systems* **2**:62–67

Foo JL, Ling H, Lee YS, Chang MW (2017) **Microbiome engineering: Current applications and its future** *Biotechnology journal* **12**

Friedlander T, Brenner N. (2009) **Adaptive response by state-dependent inactivation** *Proceedings of the National Academy of Sciences* **106**:22558–22563

Fung E, Wong WW, Suen JK, Bulter T, Sg Lee, Liao JC (2005) **A synthetic gene–metabolic oscillator** *Nature* **435**:118–122

Gomaa AA, Klumpe HE, Luo ML, Selle K, Barrangou R, Beisel CL (2014) **Programmable removal of bacterial strains by use of genome-targeting CRISPR-Cas systems** *MBio* **5**:e00928–13

Gottesman S, Roche E, Zhou Y, Sauer RT (1998) **The ClpXP and ClpAP proteases degrade proteins with carboxy-terminal peptide tails added by the SsrA-tagging system** *Genes Develop* **12**:1338–1347

Gouda MK, Manhart M, Balázsi G. (2019) **Evolutionary regain of lost gene circuit function** *Proceedings of the National Academy of Sciences of the United States of America* **116**:25162–25171 https://doi.org/10.1073/pnas.1912257116

Hiscock TW (2019) **Adapting machine-learning algorithms to design gene circuits** *BMC bioinformatics* **20**:1–13

Iman RL, Davenport JM, Zeigler DK (1980) **Latin hypercube sampling (program user's guide)** *Department of Energy, Sandia Laboratories*

Kim J, Khetarpal I, Sen S, Murray RM (2014) **Synthetic circuit for exact adaptation and fold-change detection** *Nuc Aci Res* **42**:6078–6089

Klumpp S, Hwa T. (2014) **Bacterial growth: global effects on gene expression, growth feedback and proteome partition** *Curr Opin Biotech* **28**:96–102

Klumpp S, Zhang Z, Hwa T. (2009) **Growth rate-dependent global effects on gene expression in bacteria** *Cell* **139**:1366–1375

Knox BE, Devreotes PN, Goldbeter A, Segel LA (1986) **A molecular mechanism for sensory adaptation based on ligand-induced receptor modification** *Proceedings of the National Academy of Sciences* **83**:2345–2349

Kong LW (2022) **A repository for a program using automatic differentation to find the optimal circuit parameters to achieve adaptation**

Lee HL, Shen H, Hwang IY, Ling H, Yew WS, Lee YS, Chang MW (2018) **Targeted approaches for in situ gut microbiome manipulation** *Genes* **9**

Ma W, Trusina A, El-Samad H, Lim WA, Tang C. (2009) **Defining network topologies that can achieve biochemical adaptation** *Cell* **138**:760–773

Mazyavkina N, Sviridov S, Ivanov S, Burnaev E. (2021) **Reinforcement learning for combinatorial optimization: A survey** *Computers & Operations Research* **134**

McBride C, Del Vecchio D. (2020) **The number of equilibrium points of perturbed nonlinear positive dynamical sys-tems** *Automatica* **112**

Melendez-Alvarez J, He C, Zhang R, Kuang Y, Tian XJ (2021) **Emergent Damped Oscillation Induced by Nutrient-Modulating Growth Feedback** *ACS Syn Biol* **10**:1227–1236

Melendez-Alvarez JR, Tian XJ (2022) **Emergence of qualitative states in synthetic circuits driven by ultrasen-sitive growth feedback** *PLOS Computational Biology* **18** https://doi.org/10.1371/jour-nal.pcbi.1010518

Nevozhay D, Adams RM, Van Itallie E, Bennett MR, Balázsi G. (2012) **Mapping the environmental fitness landscape of a synthetic gene circuit** *PLoS Comp Biol* **8**

Novák B, Tyson JJ (2008) **Design principles of biochemical oscillators** *Nature reviews Molecular cell biology* **9**:981–991

O'Brien EL, Van Itallie E, Bennett MR (2012) **Modeling synthetic gene oscillators** *Math Biosci* **236**:1–15

Qiao L, Zhao W, Tang C, Nie Q, Zhang L. (2019) **Network topologies that can achieve dual function of adaptation and noise attenuation** *Cell Sys* **9**:271–285

Riglar DT, Silver PA (2018) **Engineering bacteria for diagnostic and therapeutic applications** *Nature Reviews Micro-biology* **16**:214–225

Scott M, Gunderson CW, Mateescu EM, Zhang Z, Hwa T. (2010) **Interdependence of cell growth and gene expression: origins and consequences** *Science* **330**:1099–1102

Sedighi M, Zahedi Bialvaei A, Hamblin MR, Ohadi E, Asadi A, Halajzadeh M, Lohrasbi V, Mohammadzadeh N, Amiriani T, Krutova M, et al. (2019) **Therapeutic bacteria to combat cancer; current advances, challenges, and op-portunities** *Cancer medicine* **8**:3167–3181

Shen J, Liu F, Tu Y, Tang C. (2021) **Finding gene network topologies for given biological function with recurrent neural network** *Nature communications* **12**:1–10

Shi W, Ma W, Xiong L, Zhang M, Tang C. (2017) **Adaptation with transcriptional regulation** *Sci Rep* **7**:1–11

Stricker J, Cookson S, Bennett MR, Mather WH, Tsimring LS, Hasty J. (2008) **A fast, robust and tunable synthetic gene oscillator** *Nature* **456**:516–519

Strogatz SH (2018) **Nonlinear dynamics and chaos: with applications to physics, biology, chemistry, and engineering**

Tan C, Marguet P, You L. (2009) **Emergent bistability by a growth-modulating positive feedback circuit** *Nat Chem Biol* **5**:842–848

Tyson JJ, Chen KC, Novak B. (2003) **Sniffers, buzzers, toggles and blinkers: dynamics of regulatory and signaling pathways in the cell** *Current opinion in cell biology* **15**:221–231

Xia PF, Ling H, Foo JL, Chang MW (2019) **Synthetic genetic circuits for programmable biological functionalities** *Biotech-nology Advances* **37**

Zhang R, Goetz H, Melendez-Alvarez J, Li J, Ding T, Wang X, Tian XJ (2021) **Winner-takes-all resource competition redirects cascading cell fate transitions** *Nature Communications* **12** https://doi.org/10.1038/s41467-021-21125-3

Zhang R, Li J, Melendez-Alvarez J, Chen X, Sochor P, Goetz H, Zhang Q, Ding T, Wang X, Tian XJ (2020) **Topology-dependent interference of synthetic gene circuit function by growth feedback** *Nat Chem Biol* **16**:695–701

Author information

Ling-Wei Kong

School of Electrical, Computer and Energy Engineering, Arizona State University, Tempe, AZ 85287, USA

Wenjia Shi

Department of Physics, Xi'an University of Technology, Xi'an 713300, China

Xiao-Jun Tian

School of Biological and Health Systems Engineering, Arizona State University, Tempe, AZ 85287, USA
ORCID iD: 0000-0002-5601-2057

Ying-Cheng Lai

School of Electrical, Computer and Energy Engineering, Arizona State University, Tempe, AZ 85287, USA, Department of Physics, Arizona State University, Tempe, Arizona 85287, USA
For correspondence: Ying-Cheng.Lai@asu.edu
ORCID iD: 0000-0002-0723-733X

Joint Public Review:

Using computational modeling, this manuscript explores the effect of growth feedback on the performance of gene networks capable of adaptation. The authors selected 425 hypothetical synthetic circuits that were shown to achieve nearly perfect adaptation in two earlier computational studies (see Ma et al. 2009, and Shi et al. 2017). They examined the effects of cell growth feedback by introducing additional terms to the ordinary differential equation-based models, and performed numerical simulations to check the retainment and the loss of the adaptation responses of the circuits in the presence of growth feedback. The authors show that growth feedback can disrupt the gene network adaptation dynamics in different ways, and report some exceptional core motifs which allow for robust performance in the presence of growth feedback. They also used a metric to establish a scaling law between a circuit robustness measure and the strength of growth feedback. These results have important implications in the field of synthetic biology, where unforeseen interactions between designed gene circuits and the host often disrupt the desired behavior. The paper's conclusions are supported by their simulation results, although these are presented in their summary formats and it would be useful for the community if the detailed results for each topology were available as a supplementary file or through the authors' GitHub repository.

Strengths
- This work included a detailed investigation of the reasons for adaptation failure upon introducing cell growth to the systems. The comprehensiveness of the analysis makes the work stand out among studies of functional screening of network topologies of gene regulation.

- The authors' approaches for assessment of robustness, such as the survival ratio Q, can be useful for a wide range of topologies beyond adaptation. The scaling law obtained with those approaches is interesting.

Weaknesses
- The title suggests that the work investigates the 'effects of growth feedback on gene circuits'. However, the performance of 'nearly perfect adaptation' was chosen for the majority of the work, leaving the question of whether the authors' conclusion regarding the effects of growth feedback is applicable to other functional networks.

- This work relies extensively on an earlier study, evaluating only a selected set of 425 topologies that were shown to give adaptive responses (Shi et al., 2017). This limited selection has two potential issues. First, as the authors mentioned in the introduction, growth feedback can also induce emerging dynamics even without existing function-enabling gene circuits, as an example of the "effects of growth feedback on gene circuits". Limiting the investigation to only successful circuits for adaptation makes it unclear whether growth feedback can turn the circuits that failed to produce adaptation by themselves into adaptation-enabling circuits. Secondly, as the Shi et al. (2017) study also used numerical experiments to achieve their conclusions about successful topologies, it is unclear whether the numerical experiments in the present study are compatible with the earlier work regarding the choice of equation forms and ranges of parameter values. The authors also assumed that all readers have sufficient understanding of the 425 topologies and their derivation before reading this paper.

- The authors' model does not describe the impact of growth via a biological mechanism: they model growth as an additional dilution rate and calculate growth rate based on a phenomenological description with growth rate occurring at a maximum (k_g) scaled by the circuit 'burden' $b(t)$. Therefore, the authors' model does not capture potential growth rate changes in parameter values (e.g., synthetic protein production falls with increasing growth rate; see Scott & Hwa, 2023).

- The authors made several claims about the bifurcations (infinite-period, saddle-node, etc) underlying the abrupt changes leading to failures of adaptations. There is a lack of evidence supporting these claims. Both local and global bifurcations can be demonstrated with semi-analytic approaches such as numerical continuation along with investigations of eigenvalues of the Jacobian matrix. The claims based on ODE solutions alone are not sound.

- The impact of biochemical noise is not evaluated in this work; the author's analysis is only carried out in a deterministic regime.

Author Response

Joint Public Review

"Using computational modeling, this manuscript explores the effect of growth feedback on the performance of gene networks capable of adaptation. The authors selected 425 hypothetical synthetic circuits that were shown to achieve nearly perfect adaptation in two earlier computational studies (see Ma et al. 2009, and Shi et al. 2017). They

examined the effects of cell growth feedback by introducing additional terms to the ordinary differential equation-based models, and performed numerical simulations to check the retainment and the loss of the adaptation responses of the circuits in the presence of growth feedback. The authors show that growth feedback can disrupt the gene network adaptation dynamics in different ways, and report some exceptional core motifs which allow for robust performance in the presence of growth feedback. They also used a metric to establish a scaling law between a circuit robustness measure and the strength of growth feedback. These results have important implications in the field of synthetic biology, where unforeseen interactions between designed gene circuits and the host often disrupt the desired behavior. The paper's conclusions are supported by their simulation results, although these are presented in their summary formats and it would be useful for the community if the detailed results for each topology were available as a supplementary file or through the authors' GitHub repository."

We will update our GitHub repository with detailed results for each topology, along with other simulation details and results that might be of interest to the readers.

Strengths: "This work included a detailed investigation of the reasons for adaptation failure upon introducing cell growth to the systems. The comprehensiveness of the analysis makes the work stand out among studies of functional screening of network topologies of gene regulation." "The authors' approaches for assessment of robustness, such as the survival ratio Q, can be useful for a wide range of topologies beyond adaptation. The scaling law obtained with those approaches is interesting."

We are grateful to the referees and editors for their positive assessment of our work.

Weaknesses 1: "The title suggests that the work investigates the 'effects of growth feedback on gene circuits'. However, the performance of 'nearly perfect adaptation' was chosen for the majority of the work, leaving the question of whether the authors' conclusion regarding the effects of growth feedback is applicable to other functional networks."

We will change the title of the paper from "Effects of growth feedback on gene circuits: A dynamical understanding" to "Effects of growth feedback on adaptive gene circuits: A dynamical understanding," because the focus of our current work was on gene circuits with adaptation. Our work provided a framework that can be readily generalized to investigate the effects of growth feedback in other functional networks such as bistable gene circuits.

Weaknesses 2: "This work relies extensively on an earlier study, evaluating only a selected set of 425 topologies that were shown to give adaptive responses (Shi et al., 2017). This limited selection has two potential issues. First, as the authors mentioned in the introduction, growth feedback can also induce emerging dynamics even without existing function-enabling gene circuits, as an example of the "effects of growth feedback on gene circuits". Limiting the investigation to only successful circuits for adaptation makes it unclear whether growth feedback can turn the circuits that failed to produce adaptation by themselves into adaptation-enabling circuits. Secondly, as the Shi et al. (2017) study also used numerical experiments to achieve their conclusions about successful topologies, it is unclear whether the numerical experiments in the present study are compatible with the earlier work regarding the choice of equation forms and ranges of parameter values. The authors also assumed that all readers have sufficient understanding of the 425 topologies and their derivation before reading this paper."

We will make the following revisions.

1. We will modify the title of the paper as discussed above. The reviewers/editors are insightful that growth feedback could turn a non-adaptive circuit into an adaptation-enabling one - an interesting possibility worth further study.

2. We will provide details of all the pertinent numerical simulations, highlighting the differences from those in the previous work (Shi et al., 2017). Briefly, our adaptation criteria are stricter than those utilized in that work. As a result, out of the 425 topologies, random sampling based on our criteria identified adaptation in 414 topologies. For the remaining 11 topologies, either our more strict criteria have eliminated the possibility for the gene circuits to be adaptive, or the adaptive region in the high-dimensional parameter space is too small to be detected by random sampling.

3. We will describe the 425 topologies utilized in our study and provide more detail in the GitHub repository, including the topological structures and the parameter sets leading to adaptation.

> Weaknesses 3: "The authors' model does not describe the impact of growth via a biological mechanism: they model growth as an additional dilution rate and calculate growth rate based on a phenomenological description with growth rate occurring at a maximum (kg) scaled by the circuit 'burden' b(t). Therefore, the authors' model does not capture potential growth rate changes in parameter values (e.g., synthetic protein production falls with increasing growth rate; see Scott & Hwa, 2023)."

We considered dilution due to cell growth as the dominant factor of growth feedback. In fact, we studied the adaptive circuits without growth and their ability to maintain their adaptive behaviors after dilution into a fresh medium, based on a recent work [Zhang, et al., Nature Chemical Biology 16.6 (2020): 695-701]. A higher growth rate can change synthetic protein production. However, the dynamic roles of the dilution and growth-affected production rate should be analogous, given that they both act as inhibitory factors arising from cell growth as mentioned by the reviewers/editors. Taking the growth effect on the production rate into account would require a more comprehensive study. We will elaborate on the limitation of our modeling framework and include the pertinent references (e.g., Scott & Hwa, 2023).

> Weaknesses 4: "The authors made several claims about the bifurcations (infinite-period, saddle-node, etc) underlying the abrupt changes leading to failures of adaptations. There is a lack of evidence supporting these claims. Both local and global bifurcations can be demonstrated with semi-analytic approaches such as numerical continuation along with investigations of eigenvalues of the Jacobian matrix. The claims based on ODE solutions alone are not sound."

We will add this material to our next version of the paper. A further semi-analytic analysis can better justify the numerically discovered bifurcations.

> Weaknesses 5: "The impact of biochemical noise is not evaluated in this work; the author's analysis is only carried out in a deterministic regime."

Our work focused on uncovering the deterministic dynamical mechanisms underlying growthfeedback induced circuit failures in situations where all protein concentrations are high so that neglecting the effects of biochemical noises can be justified. Incorporating noises into our analysis will significantly complicate the study and likely prevent the dynamical origin of the failures from being unveiled. Nonetheless, the effects of biochemical noises are important and we will provide a discussion in the revised manuscript.